Cell age, not chronological age, governs the dynamics and longevity of circulating $CD4^+$ memory T cells

M. Elise Bullock[1]¤, Thea Hogan[2]¤, Sinead Morris[1], Maria Nowicka[1], Christiaan van Dorp[1], Andrew J. Yates[1]‡*, Benedict Seddon[2]‡*

[1] Department of Pathology and Cell Biology, Columbia University Irving Medical Center, 630 West 168th Street, New York, NY 10032, USA
[2] Institute of Immunity and Transplantation, Division of Infection and Immunity, UCL, Royal Free Hospital, Rowland Hill Street, London NW3 2PF, United Kingdom

¤ Contributed equally

‡ Contributed equally

*Address correspondence to either author; andrew.yates@columbia.edu, benedict.seddon@ucl.ac.uk

Abstract

Quantifying the kinetics with which memory T cell populations are generated and maintained is essential for identifying the determinants of the duration of immunity. The quality and persistence of circulating $CD4^+$ effector memory (T_{EM}) and central memory (T_{CM}) T cells in mice appear to shift with age, but it is unclear whether these changes are driven by the aging host environment, by cell age effects, or both. Here we address these issues by combining DNA labelling methods, an established fate-mapping system, and mathematical models. Together these allow us to quantify the dynamics of both young and established circulating memory $CD4^+$ T cell subsets, within both young and old mice. We find strong evidence that cell-age effects dominate host-age effects, and that clones become more quiescent and more persistent the longer they reside within the T_{CM} and T_{EM} pools. This behaviour will lead to an increasingly long-tailed distribution of clone sizes as an individual ages. Therefore, the age structure of $CD4^+$ T_{CM} and T_{EM} clones can explain bulk changes in their dynamics and persistence across the lifespan.

Keywords: memory T cells, busulfan chimeric mice, mathematical modelling

Author Summary

Our long-term protection against infections depends in part on the maintenance of diverse populations of CD4 memory T cells, which are made in response to the initial exposure to the pathogen or a vaccine. These cells are not long-lived, but instead are maintained dynamically at a clonal level through loss and division. Understanding how immune memory persists therefore requires measuring these rates of these processes, and how they might change with age. Here we combine mouse experiments with mathematical models to show that CD4 memory T cell clones have a complex dynamical structure but become progressively more quiescent with time. Their expected cell lifespan increases as they age, leading to long-tailed survival curves. This dynamic implies that as individuals age, their CD4 memory populations become enriched for older clones that have a fitness advantage over newly generated ones. If these older clones are functionally impaired, this phenomenon may contribute to the waning of immunity in the elderly.

Introduction

$CD4^+$ T cells can suppress pathogen growth directly and coordinate the activity of other immune cells [1, 2]. Following exposure to antigen, heterogeneous populations of circulating memory CD4 T cells are established that enhance protection to subsequent exposures. In mice, these can be categorised broadly as central (T_{CM}) or effector (T_{EM}) memory. Canonically defined T_{CM} have high expression of CD62L, which allow them to circulate between blood and secondary lymphoid organs, while CD4 T_{EM} express low levels of CD62L and migrate to tissues and sites of inflammation. The lineage relationships between CD4 T_{CM} and T_{EM}, and other memory CD4 subsets, remain unclear [3].

In mice, circulating memory CD4 T cells appear not to be intrinsically long-lived, but are lost through death or onward differentiation on timescales of days to weeks [4–9]. However, compensatory self-renewal can act to sustain memory T cell clones, defined as populations sharing a given T cell receptor (TCR), for much longer than the lifespan of their constituent cells [10]. To understand in detail how the size of memory T cell populations change with time since exposure to a pathogen, we therefore need to be able to quantify their rates of *de novo* production, division, and loss, any heterogeneity in the rates of these processes, how kinetically distinct subsets are related, and how their kinetics might change with host and/or cell age.

Much of our knowledge of memory CD4 T cell dynamics derives from studies of laboratory mice housed in specific pathogen-free conditions who have not experienced overt infections, but nevertheless have abundant memory phenotype (MP) CD4 T cells [11–13]. These populations contain both rapidly dividing and more quiescent populations [4, 14–17], a stratification that holds within the T_{CM} and T_{EM} subsets [5]. MP T cells are established soon after birth, and attain broadly stable numbers determined in part by the cleanliness of their housing conditions [18]. After the first few weeks of life, however, both CD4 T_{CM} and CD4 T_{EM} are continuously replaced at a rates of a few percent of the population size per day [5], independent of environment [18]. MP CD4 T cells are therefore likely specific for an array of environmental, commensal and self antigens, and may comprise subpopulations at different stages of maturation or developmental end-points. Dissecting their dynamics in detail may then shed light on the life-histories of conventional memory cells induced by infection.

A widely-used approach to studying lymphocyte population dynamics is DNA labelling, in which an identifiable agent such as bromodeoxyuridine (BrdU) or deuterium is taken up during cell division. By measuring the frequency of cells within a population that contain the label during and following its administration, one can use mathematical models to extract rates of production and turnover (loss). Without allowing for the possibility variation in these rates within a population, their average estimates may be unreliable [19, 20]. Explicit treatment of such 'kinetic heterogeneity' can yield estimates of average production and loss rates that are interpretable and independent of the labelling period, although the number of distinct subsets and the lineage relationships between them are difficult to resolve [4, 5, 18, 21]. Further, models of labelling dynamics usually conflate the processes of influx of new cells and self-renewal of existing ones into a single rate of cell production. Distinguishing these processes is particularly important in the context of memory, because their relative contributions determine the persistence of clones within a population; for a population at equilibrium, clones are diluted by influx, but sustained by self-renewal.

To address these uncertainties, one can combine DNA labelling with information from other systems to validate predictions or constrain the choice of models. One approach is to obtain an independent estimate of any constitutive rate of flow into a population by following its replacement by labelled precursors. In a series of studies, we established a mouse model that yields the rates of replacement of all peripheral lymphocyte subsets at steady state [5, 18, 22–27]. In this system, illustrated in Fig 1A, low doses of the transplant conditioning drug busulfan are administered to specifically deplete hematopoietic stem cells (HSC) in adult mice, while leaving peripheral lymphocyte compartments undisturbed. Shortly afterward, the treated mice receive T and B cell-depleted bone marrow from congenic donors, to reconstitute the HSC niche. Donor fractions of 70-90% are established rapidly among HSC, which are stable long-term [22]. Within six weeks of transplant, the fraction of cells that are donor-

derived (the chimerism) equilibrates at similar levels at all stages of thymic development and at the transitional stage of B cell development, indicating that turnover of all these populations is complete within this time frame [22]. Donor-derived cells proceed to gradually replace host-derived cells in all peripheral lymphocyte compartments over timescales of weeks to months, while leaving total cell numbers indistinguishable from untreated controls [5]. By using mathematical models to describe the timecourse of replacement within a particular population, one can obtain a direct estimate of the rate of influx of new cells, which can be fed directly into models of DNA labelling [5]. A conceptually similar approach to measuring influx is to use division-linked labelling to explicitly model the kinetics of label in both the population of interest and its precursor. This method is particularly useful when labelling is inefficient, because labelling among precursors is not saturated and is time-varying. Their influx then leaves an informative imprint on any labelling within the target population itself, allowing the rate of ingress of new cells to be inferred [28].

Another means of boosting the resolving power of DNA labelling assays is to use concurrent measurements of Ki67, a nuclear protein expressed during mitosis and for a few days afterwards [22, 29, 30]. A cell's BrdU content and Ki67 expression then report its historical and recent division activity, respectively. This approach was used to study MP CD4 T cell dynamics [5] and rule out a model of 'temporal heterogeneity', in which CD4 T_{CM} and T_{EM} cells each comprise populations of cells that divide at a uniform rate, but each cell's risk of loss varies with the time since it last divided. The BrdU/Ki67 approach instead supported a model in which CD4 T_{EM} and T_{CM} each comprise at least two kinetically distinct ('fast' and 'slow') subpopulations, consistent with other studies [4, 16, 17]. These subpopulations were assumed to form independent lineages that branch from a common precursor [5], but a subsequent study using the busulfan chimera system alone found support for an alternative model in which memory cells progress from fast to slow behaviour [18]. The topologies of the kinetic substructures of CD4 T_{CM} and T_{EM} therefore remain uncertain.

Here, we aimed to characterise the dynamics CD4 T_{CM} and T_{EM} in full, by combining these two approaches – performing BrdU/Ki67 labelling within busulfan chimeric mice directly. Our reasoning was threefold. First, if one defines a memory cell's age as the time since it or its ancestor entered the memory pool, the average age of donor (newly recruited) clones will be lower than that of the host-derived clones that they are replacing. By stratifying the BrdU/Ki67 analyses by donor and host cells one can therefore quantify any changes in the kinetics of memory T cell clones with their age. Second, by performing the labelling experiments in young and aged cohorts of mice, one can simultaneously observe any changes in dynamics due to the mouse's chronological age. Third, we hoped that this combined approach would allow us to define the relationship between fast and slow memory CD4 T subsets, and identify the immediate precursors of MP CD4 T_{CM} and T_{EM}.

Results

Performing DNA labelling assays in busulfan chimeric mice

We studied two age classes of mice (Fig 1B). In one cohort, mice underwent busulfan treatment and bone marrow transplant (BMT) aged between 58 and 116 days and BrdU/Ki67 labelling was performed 56-91 days later (aged between 150-175 days). For brevity we refer to these as 'young' mice. An 'old' cohort underwent treatment and BMT at similar ages, but with labelling performed between 246 and 260 days later (aged between 304 and 341 days). BrdU was administered by intraperitoneal injection and subsequently in drinking water for up to 21 days. Mice were sacrificed at a range of time points within this period, or up to 14 days after BrdU administration stopped. CD4 T_{CM} and T_{EM} were recovered from lymph nodes and enumerated (Fig 1C; see Methods for details).

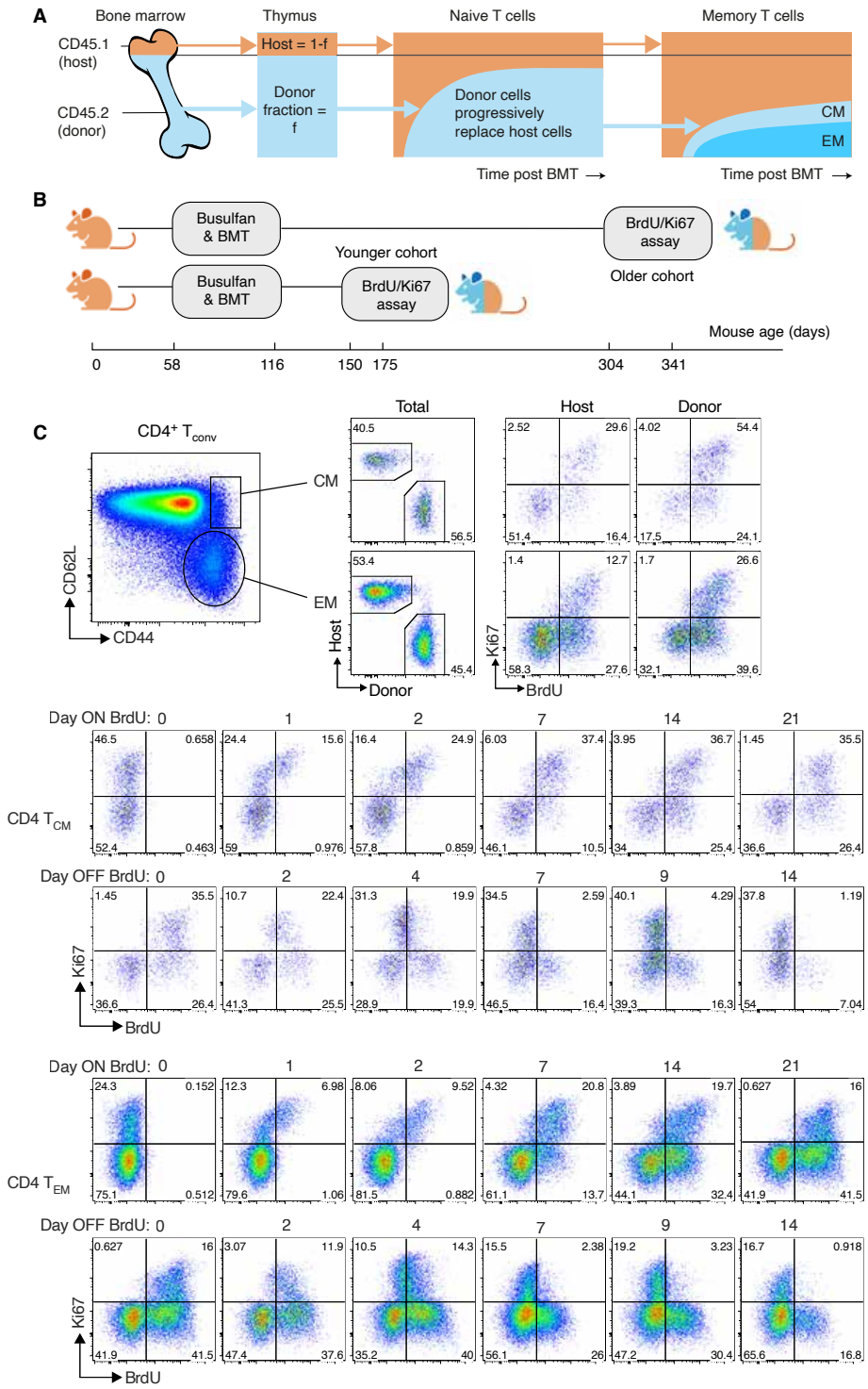

Figure 1 – Busulfan chimeric mice, experimental design and gating strategies. A Schematic of the busulfan chimeric mouse system, adapted from ref. 31. **B** Design of the BrdU/Ki67 labelling assay, studying two cohorts at different times post BMT. **C** Flow plots illustrate the gating strategy used to identify CD44^{hi} CD62L^{hi} CD4 T_{CM} and CD44^{hi} CD62L^{lo} CD4 T_{EM} subsets, and CD45.1 (host) and CD45.2 (donor) subsets within. Chimeric mice were fed BrdU for 21 days. Mice were analysed at different times during feeding, and across 14 days following its cessation. Here we show a representative example of Ki67 and BrdU staining stratified by donor and host, and CD4 T_{CM} and CD4 T_{EM}. Timecourses show Ki67 BrdU labelling during BrdU feeding (ON BrdU), and in the chase period (OFF BrdU), among CD4 T_{CM} and CD4 T_{EM}.

The proliferative activity of CD4 T_{CM} and T_{EM} clones declines as they age

We first analyzed the bulk properties of CD4 MP T cells within the two cohorts. The total numbers of CD4 T_{CM} and T_{EM} recovered from lymph nodes increased slightly with age (Fig 2A). Proliferative activity, measured by the proportion of cells expressing Ki67 (Fig 2B), fell slightly with age among CD4 T_{CM} (median $Ki67^{high}$ fraction = 0.44 in young cohort, 0.36 in older cohort, p =0.02) but not significantly for T_{EM} (median $Ki67^{high}$ fraction = 0.20 in both age groups, p =0.48).

Consistent with reports of the production of new MP CD4 T cells throughout life [5, 18], and the progressive enrichment of all T cell subsets in donor-derived cells after BMT, the composition of both memory subsets shifted towards donor cells in older mice (Fig 2C). This shift was more marked for T_{CM} ($p < 10^{-4}$) but was also significant for T_{EM} ($p < 10^{-3}$). Strikingly, in the younger cohort, donor T_{CM} and T_{EM} both expressed Ki67 at substantially higher frequencies than their host counterparts (Fig 2D; $p < 10^{-8}$ in both cases). These differences diminished with time post BMT but remained significant in the older cohort ($p < 10^{-3}$ for both T_{CM} and T_{EM}).

These patterns of donor/host cell differences indicate that the average levels of proliferation within cohorts of CD4 T_{CM} and T_{EM} decline with the time since they or their ancestors entered the population. This effect is strongly apparent among T_{CM} but still appreciable for T_{EM}.

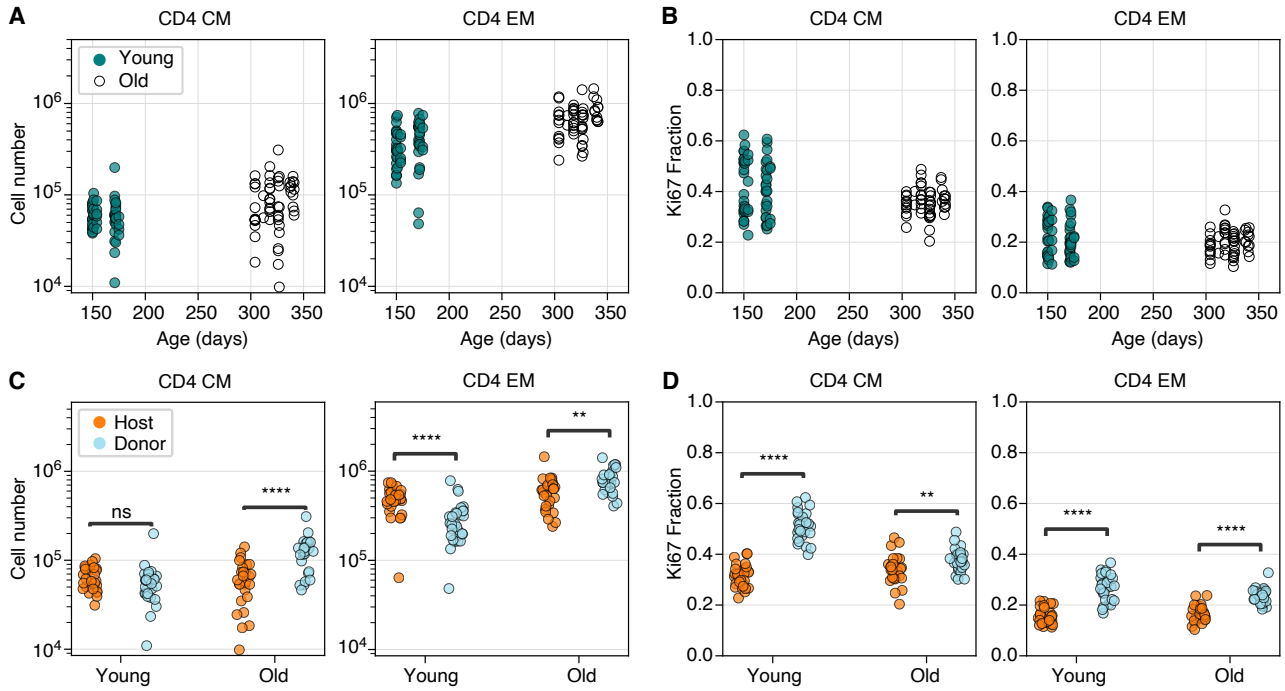

Figure 2 – Busulfan chimeric mice reveal shifts in CD4 memory T cell dynamics with both mouse age and cell age. A, B: Numbers and Ki67 expression levels of CD4 T_{CM} and T_{EM} recovered from lymph nodes in young and old cohort (Mann-Whitney tests). **C, D:** Numbers and Ki67 expression levels of CD4 T_{CM} and T_{EM} in young and old mice, stratified by average cell age (host and donor; Wilcoxon tests). ** $p < 10^{-3}$; *** $p < 10^{-4}$; **** $p < 10^{-5}$.

Modelling BrdU/Ki67 labelling kinetics in busulfan chimeric mice

To find a mechanistic explanation of these patterns, we then analysed the BrdU/Ki67 timecourses derived from the young and old mice. As described in Methods, and illustrated in Fig 1B, in each age cohort we followed the uptake and loss of BrdU within CD4 T_{CM} and T_{EM}, stratified by host and donor cells and by Ki67 expression, during 21 day pulse and 14 day chase periods. This strategy allowed us to isolate the dynamics of new and old

memory cells within young and old mice.

We attempted to describe these data using three classes of mathematical model, shown schematically in Fig 3A. The temporal heterogeneity (TH) model assumed that each memory subset (T_{CM}/T_{EM}, host/donor) divides at its own uniform rate, but that Ki67^{high} cells, which are actively dividing or divided recently, are lost at a different rate to that of more quiescent Ki67^{low} cells. This is an instance of a more general model in which a cell's risk of death changes with the time since its last division [32]. Our TH model is itself a simple generalisation of a purely homogeneous model in which cells divide and die at constant, uniform rates, independent of their expression of Ki67. Previously we found little evidence for the TH model when studying the dynamics of CD4 T_{CM} and T_{EM} in bulk [5], but we considered it again here to validate that conclusion. We also employed two versions of a kinetic heterogeneity (KH) model; branched, in which newly generated T_{CM} and T_{EM} both immediately bifurcate into independent subpopulations (A and B) with distinct rates of division and death [5], and linear, in which cells enter memory with phenotype A and mature into a kinetically distinct phenotype B [18] (Fig 3A, models (ii) and (iii)). In both linear and branched models, new cells entering the memory pool are assumed to be Ki67^{high}, reflecting the assumption that they have recently undergone clonal expansion.

We encoded these models with systems of ordinary differential equations. The core structure, which describes the flows between BrdU$^{\pm}$ and Ki67$^{high/low}$ cells as they divide and die during the labelling period, is illustrated in Fig 3B. A detailed description of the formulation of the models is in S1 Text.

Within both cohorts of mice, the total numbers of host and donor CD4 T_{CM} and T_{EM} cells, and the frequencies of Ki67^{high} cells within each, were approximately constant over the course of the labelling assays (Fig S1). We therefore made the simplifying assumption that both donor and host memory populations were in quasi-equilibrium, with any changes in their numbers or dynamics occurring over timescales much longer than the 35 day labelling experiment. We took a Bayesian approach to estimating model parameters and performing model selection, using Python and Stan, which is detailed in S2 Text. The code and data needed to reproduce our analyses and figures can be found at `github.com/elisebullock/tcellmemorypaper`.

Branched and linear models of memory CD4 T cell dynamics can both explain BrdU/Ki67 labelling kinetics

The BrdU labelling data are summarised in Figs 3C and D, shown as the accumulation and loss of BrdU within each population as a whole (left hand panels) and within Ki67^{high} and Ki67^{low} cells (centre and right panels). In the young cohort (Fig 3C), the labelling kinetics of more established (host) and more recently generated (donor) CD4 T_{CM} and T_{EM} were quite distinct, with slower BrdU uptake within host-derived populations. In addition, heterogeneity was apparent in all labelling timecourses. For a kinetically heterogeneous population, the slope of this curve then declines as the faster-dividing populations become saturated with label, and the majority of new uptake occurs within cells that divide more slowly. Such behaviour was apparent, consistent with the known heterogeneity in rates of division and/or loss within both T_{CM} and T_{EM}. In the older cohort (Fig 3D) BrdU uptake was slower, differences between donor and host kinetics were less apparent, and the labelling kinetics of host-derived cells were similar to those in the younger cohort.

Intuitively, the initial rate of increase of the BrdU-labelled fraction in a population will depend both on the mean division rate of the population and the efficiency of BrdU incorporation per division, [33]. In general this efficiency, which we denote ϵ, is unknown and this uncertainty confounds the estimation of other parameters [33, 34]. In this regard, the timecourses of the proportion of Ki67^{high} cells that are BrdU-positive (Fig 3C and D, centre panels) are highly informative. Any deviation from a rapid increase to 100% places bounds on ϵ, and as we see below, the posterior distributions of this parameter were narrow. Similarly, the kinetics of the BrdU-positive fraction within Ki67^{low} cells are highly informative regarding the lifetime of Ki67 expression – we expect this lifetime to be the delay before the first BrdU-positive Ki67^{low} cells appear, which is clearly apparent in the data (Figs 3C and D, right hand panels) and was again tightly constrained in the model fitting.

To test whether all the parameters of the models illustrated in Fig 3A were identifiable, we fitted each to simulated BrdU/Ki67 labelling timecourses that were generated by the model with added noise. For all models, the estimated total rate of influx of new cells into memory was strongly correlated with the net loss rate of the direct descendant(s) of the source, indicating that these parameters are not separately identifiable. To resolve this, we obtained independent estimates of the rates of influx by modelling the slow accumulation of donor CD4 T_{CM} and T_{EM} within cohorts of busulfan chimeric mice over long timescales (S3 Text, Fig S2). The posterior distributions of these estimates (summarised in Table S1) yielded strong priors on the influx rates for the subsequent analyses.

We fitted the three models to each of the eight timecourses – CD4 T_{CM} and T_{EM} separately for donor and host, in both young and old cohorts. The TH models performed poorly (Fig S3), while the branched and linear models both yielded excellent fits to the data. Surprisingly, these fits were statistically and visually indistinguishable (ELPD differences with standard errors; T_{CM} donor 0.016 (0.37); T_{CM} host 0.078 (0.41); T_{EM} donor 2.8 (0.86); T_{EM} host 0.16 (0.59)). However, parameters estimated for the linear model exhibited greater co-linearity (Fig S4A), so we proceed by describing the branched model, whose parameters were more clearly identifiable (Fig S4B). The fits of the branched model are overlaid in Fig 3C. The posterior distributions of its parameters are shown in Fig 4 and summarised in Table S2. Corresponding results for the linear model are shown in Figs S5 and S6. Importantly, however, the conclusions we draw from here onwards are supported by both models. We return to the issue of discriminating between the branched and linear topologies below.

Clonal age effects expain changes in CD4 T_{CM} and T_{EM} dynamics with mouse age

For both CD4 T_{CM} and T_{EM}, the branched model fits indicated that in both young and older mice, cells that enter the faster subpopulation from the precursor pool divided and were lost over timescales of a few days. In contrast, slow cells divided rarely (mean interdivision times of 100-200 days) and had lifespans of 60-100 days (Fig 4). While the differences in these two subpopulations are clear, these division and loss rate estimates are rather broad because they still exhibited some co-linearity (Fig S4B). We return to the issue of estimating average cell lifetimes below. Quantities that were better defined, and perhaps immunologically more relevant, were the balance of loss (at rate δ) and self-renewal (at rate α) for each subpopulation. This net loss rate, $\lambda = \delta - \alpha$, defines the half life of a clonal population, $\ln 2/\lambda$ (for example, if the rate at which cells are lost is is balanced exactly by self renewal, $\lambda = 0$ and the clone is sustained indefinitely). The similarity in the rates of division and loss of fast cells implied that fast CD4 T_{CM} and T_{EM} clones were remarkably persistent, with half lives of between 35-70 days, and T_{EM} slightly less persistent than T_{CM}. In contrast, the slower clones self-renewed rarely, and so their half-lives (70-140 days) were governed largely by cell lifespan, and were similar for T_{CM} and T_{EM}.

Going beyond these broad characterisations, we sought to use the parameter estimates to identify the basis of the observed host/donor differences, and the changes in dynamics with mouse age. In particular, in young mice, for both T_{CM} and T_{EM}, the model fits reproduced the higher expression of Ki67 within donor cells and indicated that both subsets possessed substantially higher proportions of fast cells than their host counterparts (Fig 4). To understand the basis of this difference, we derived an expression for the proportion of a memory population that is fast cells, p_A, in the branched model:

$$p_A^{\text{branched}} = \frac{1}{1 + \left(\frac{1-f_A}{f_A}\right) \lambda_A/\lambda_B}, \tag{1}$$

where f_A is the proportion of the source entering the fast population, which was slightly lower for T_{EM} than T_{CM} (Fig 4). For both subsets we saw no significant differences in f_A between host and donor cells or between young and old mice, indicating that for each subset the rationing of new memory cells into fast and slow subsets was an invariant quantity. The differences in the donor/host fast fractions must therefore derive from the ratio of fast to slow clonal loss rates, λ_A/λ_B. In young mice, fast donor T_{CM} clones were marginally less persistent

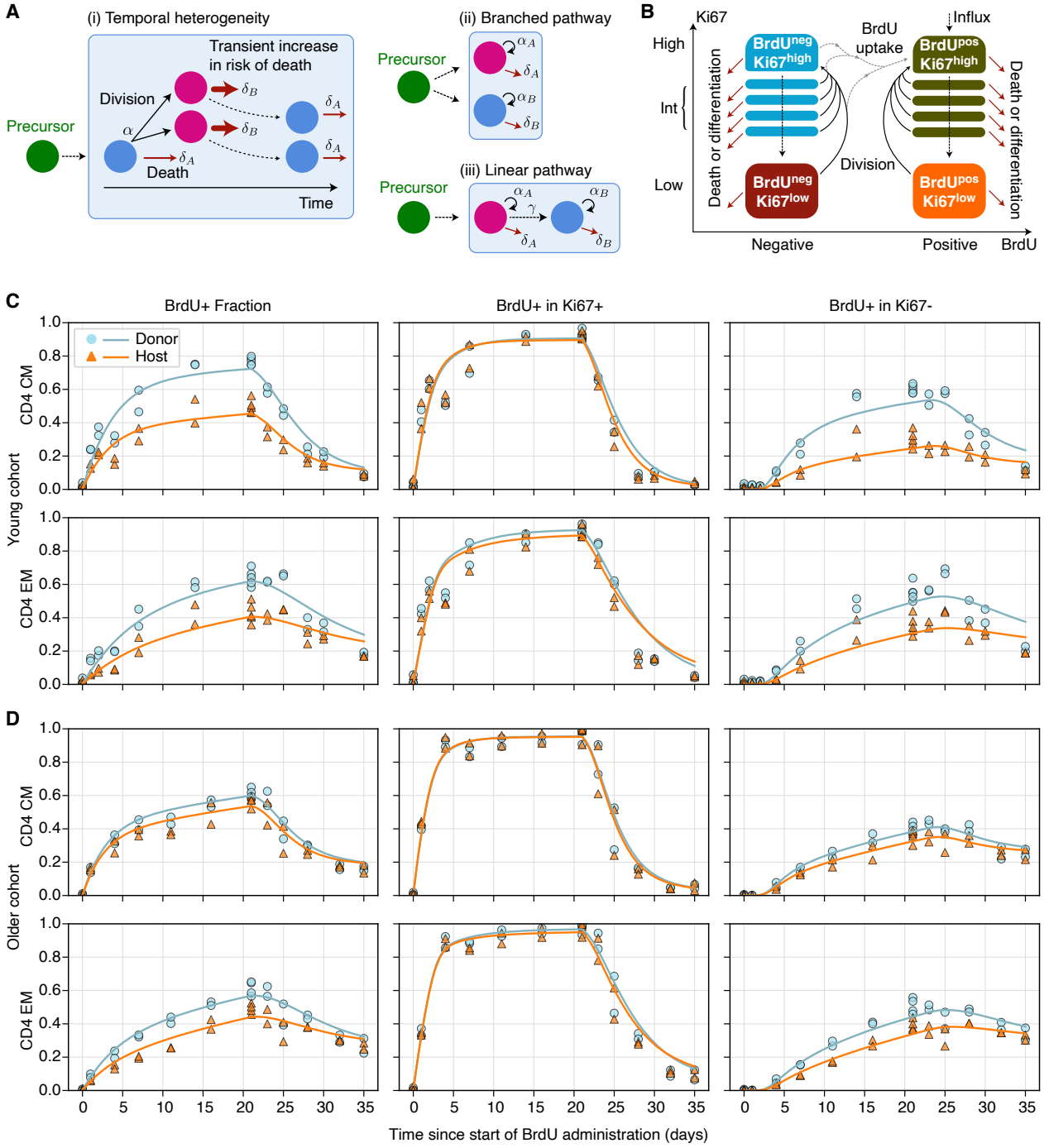

Figure 3 – Modelling BrdU/Ki67 timecourses. **A** Models of heterogeneity in cellular dynamics within a memory subset. Adapted from ref. [31]. **B** Schematic of the core component of the ODE model used to describe the uptake of BrdU and the dynamic of Ki67 expression. **C-D** Fitted kinetics of BrdU uptake and loss in CD4 T_{CM} and T_{EM}, in the young (**C**) and older (**D**) cohorts of mice. The left column shows the frequency of BrdU-positive cells within donor and host cells. Centre and left columns show the proportion of BrdU-positive cells within Ki67-positive and Ki67-negative cells respectively.

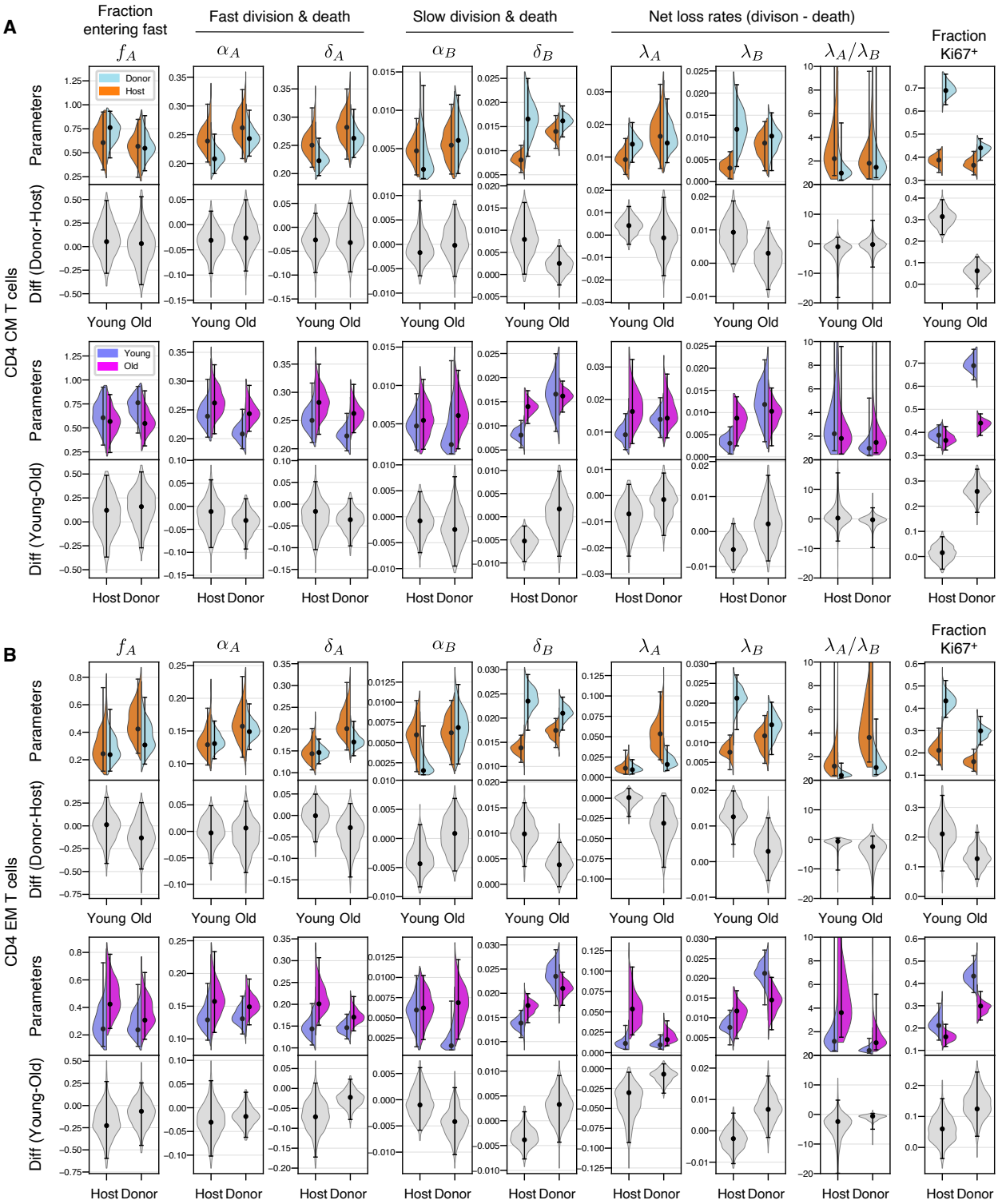

Figure 4 – Posterior distributions of parameters derived from the branched model of the kinetics of CD4 T_{CM} (**A**) and T_{EM} (**B**), in the young and old cohorts of mice. Grey violin plots show differences in parameters (host/donor, and young/old). Points and bars show MAP estimates and 95% credible intervals, respectively.

than host counterparts ($\lambda_A^{\text{donor}} \gtrapprox \lambda_A^{\text{host}}$) but slow donor clones were much less persistent than slow host clones ($\lambda_B^{\text{donor}} > \lambda_B^{\text{host}}$). Thus, for T_{CM}, λ_A/λ_B was smaller for donor than host, leading to a greater fast cell fraction and so explaining the donor-skewed Ki67 fraction (Fig 2). For T_{EM} the picture was similar; in the younger cohort, clonal lifespans of fast cells were similar for donor and host, but slow donor clones were substantially shorter lived than host clones. Therefore, again, λ_A/λ_B was smaller for donor than host. In older mice, all differences in parameters between host and donor cells shrank, although the fast fraction remained significantly higher for donor in both T_{CM} and T_{EM}. These patterns reflected the degree of convergence of Ki67 expression of host and donor cells (Fig 2D).

We expected the age structure of host-derived CD4 T_{CM} and T_{EM} to change between young and old cohorts to a lesser extent than that of the donor cells. Therefore, any changes linked directly to mouse age ought to be more manifest in host cell dynamics. However we saw no shifts in either the fast or slow clonal loss rates of host cells between the age cohorts, reflected in the similarity of the BrdU/Ki67 labelling curves in host cells in young and old mice (Fig 3, panels C and D).

We can draw two conclusions from these observations. First, because donor memory cells are younger on average than host cells, differences in their kinetics in younger mice are readouts of the effects of cell age. Consistent with this, their convergent dynamics in older mice reflect a convergence in host and donor cell age profiles. As they age, slow T_{CM} and T_{EM} clones become substantially longer lived, shifting the population as a whole to a more quiescent and persistent state. This increase in clonal persistence appears to derive from better survival, rather than any increase in self renewal. Second, the invariance of host cell dynamics across the two age groups indicates that the observed changes in the bulk behaviour of T_{CM} and T_{EM} as mice age derive largely from cell-age-dependent changes in clonal persistence, rather than any cell-extrinsic effects relating to the age of the mouse.

These conclusions also held for the linear model. There, the fraction of the population made up of fast cells is given by the simpler expression

$$p_A^{\text{linear}} = \frac{1}{1 + \gamma/\lambda_B}, \tag{2}$$

where γ is the rate of differentiation or maturation from fast (A) to slow (B). We saw no differences in γ between host and donor, or across mouse age (Fig S6). In contrast, λ_B for donor cells was higher than for host cells in young mice, again explaining the higher fast fraction among donor cells and hence their higher Ki67 expression. In older mice, the loss rate of slow donor clones approached that of host clones, yielding the same conclusion drawn from the branched model.

Comparing memory CD4 T cell lifespans to previous estimates

The other DNA labelling studies we are aware of that measured or inferred memory CD4 T cell lifespans in mice reported the population average, and did not distinguish T_{CM} and T_{EM} [4, 8, 33]. For comparison, we used three independent methods of deriving the corresponding mean lifespan from our data.

Westera *et al.* [4], using heavy water labelling, showed that it is necessary to allow for multiple subpopulations with different rates of turnover to obtain parameter estimates that are independent of the labelling period. They were not able to resolve the number of subpopulations or their rates of turnover individually, but established a robust estimate of the mean lifespan of 15 days (range 11-15) in adult mice. Baliu-Pique *et al.* [8] employed the same approach to derive a lifespan of 8 days (95% CI 5-15). To obtain an analogous estimate, we used the model parameters to calculate the average loss rate of fast and slow cells among both donor and host, each weighted by their population sizes (S4 Text). Fig 5A shows the posterior distributions of the lifespans of T_{CM} and T_{EM} separately, with point estimates of roughly 8 and 21 days respectively, and with little change with mouse age. Notably, our confidence in these quantities is greater than our confidence in the lifespans of fast and slow populations themselves (Fig 4). To calculate a population-average lifespan, we account for the lower prevalence

of T_{CM} relative to T_{EM} (Fig 5B). The resulting weighted estimates were 18 days (95% CrI 16-21) for younger mice, and 20 days (18-22) in the older cohort (Fig 5C).

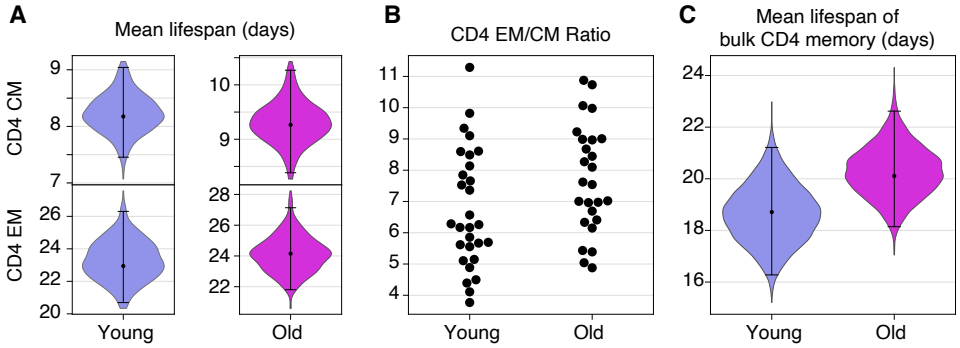

Figure 5 – Estimating the mean lifespan of circulating memory CD4 T cells in mice. **A** Expected lifespans of CD4 T_{CM} and T_{EM} in young and old mice, each averaged over fast and slow subpopulations, calculated using Eq 2. **B** Relative frequency of lymph node-derived CD4 T_{CM} and T_{EM}, by age. **C** Estimated mean lifespans of memory CD4 T cells, averaging over T_{CM} and T_{EM}, in the young and old cohorts.

We can obtain approximate estimates of the mean lifespan of memory CD4 T cells in two other ways. Both rely on estimating the total rate of production, which at steady state balanced by the average loss rate, which is the inverse of the mean lifespan. One method is to use the initial upslope of the BrdU labelling curve, which reflects the rate of production of cells through division and influx. One can show that the mean lifespan is approximately $2\epsilon/p$, where ϵ is the efficiency of BrdU uptake and p is the early rate of increase of the $BrdU^+$ fraction (S5 Text). In the young cohort, these rates were roughly 0.08/day and 0.04/day for T_{CM} and T_{EM} respectively; in older mice, 0.1 and 0.05. Accounting again for the T_{CM} and T_{EM} abundances (Fig 5B), we obtain rough point estimates of the lifespan of 25 days in the younger cohort and 27 days in the older mice. A similar calculation was employed by De Boer and Perelson [33], who drew on BrdU labelling data from Younes *et al.* [17] to obtain a mean lifespan of between 14 and 22 days (S5 Text for details).

The second method is to utilise Ki67 expression, which reflects the production of cells through both influx and cell division. If the fraction of cells expressing Ki67 is k, and Ki67 is expressed for T days after division, one can show that the mean lifespan is approximately $-T/\ln(1-k)$ (S5 Text). The frequencies of Ki67 expression within CD4 T_{CM} and T_{EM} were roughly 0.4±0.1 and 0.2±0.1 respectively, and were similar in young and old mice (Fig 2B); using these values weighted by the abundances of T_{CM} and T_{EM} (Fig 5B) gives a mean lifespan of approximately 12 days (range 9-26).

In summary, we find consistent estimates of the average lifespan of memory CD4 T cells in mice that change little with age and are in line with estimates from other studies.

Using patterns of chimerism to identify the precursors of CD4 T_{CM} and T_{EM}

These models of CD4 T_{CM} and T_{EM} dynamics made no assumptions about the identity of their precursors – they only assumed that the rates of influx of host and donor precursors into each subset were constant over the course of the labelling assay, and that new memory cells expressed Ki67 at high levels. Because the donor/host composition of this influx presumably reflects the chimerism of the precursor population, we reasoned that by comparing the chimerism of the flows into CD4 T_{CM} and T_{EM} to that of other populations we might construct a map of the differentiation of CD4 MP T cell subsets.

Fig 6 shows these chimerism estimates. Those inferred from modelling are shown with violin plots (derived from the posterior distributions of parameters in both the branched and linear models), and the points represent experimental observations. Our analysis of the rate of accumulation of donor cells within CD4 T_{CM} and T_{EM} in

busulfan chimeric mice (Eq 1 and Fig S2) yielded the chimerism of the flows into these subsets, shown on the left (CM Source and EM Source).

As expected, chimerism in different cell populations showed considerably more variation in the young cohort, which had undergone BMT relatively recently, than in the older cohoxhich donor/host ratios throughout the peripheral T compartments had had more time to approach equilibrium. We therefore focused on the younger cohort to establish potential differentiation pathways. We also saw very little difference in the parameter estimates derived from the branched and linear models, indicating that our inferences are robust to the choice of model.

One source of new memory might be antigen-specific recent thymic emigrants (RTE), whose chimerism is similar to that of early-stage double positive thymocytes (DP1). However, the chimerism of DP1 cells was much higher than the chimerism of the T_{CM} or T_{EM} precursors, so our analyses do not support RTE as the dominant source of new CD4 MP T cells. Instead, the chimerism of T_{CM} precursors aligned well with that of bulk naive CD4 T cells; and the chimerism of the T_{EM} precursors aligned with that of T_{CM}. This pattern clearly suggests a naive $\rightarrow T_{CM} \rightarrow T_{EM}$ developmental pathway for CD4 MP T cells. Notably, this pathway is consistent with the order in which donor-derived cells appear within these subsets in busulfan chimeras (Fig S2). The modelling also provided a breakdown of the observed chimerism of CD4 T_{CM} and T_{EM} into the fast and slow components. It was clear that the estimated chimerism within the slow cells was too low for them to be an exclusive source for any other population, consistent with their being predominantly a terminal differentiation stage in memory T cell development. Instead, any CD4 T_{CM} feeding the T_{EM} pool are likely derived largely from the faster-dividing T_{CM} subpopulation.

Age-dependent survival rates explain shortfalls in replacement within T_{CM} and T_{EM}

In older busulfan chimeric mice, the replacement curves for CD4 T_{CM} and T_{EM} saturate at donor fractions of approximately 0.7 and 0.6 respectively (Fig S2 and Fig 6), lower than that of naive CD4 T cells (Fig 6). Given the short average lifespans of CD4 T_{CM} and T_{EM}, implying rapid turnover of both subsets, it is then perhaps puzzling that the donor fractions within all three compartments do not equalise at late times after BMT. Our analysis suggests that these shortfalls are an effect of cell-age-dependent survival. The mean lifespan is a rather crude measure of memory turnover, as lifespans are significantly right-skewed; in addition, slower cells increase their life expectancies as they age. This increase will lead to a first-in, last-out effect; donor T cell clones will always be at a survival disadvantage, on average, relative to their older host counterparts. This effect naturally leads to a shortfall in the donor fraction relative to the precursor (putatively, T_{CM} relative to naive; and T_{EM} relative to T_{CM}). As the mice age and the donor and host cell age distributions converge, this shortfall decreases, but still remains (Fig 6).

Limitations of Ki67 information for establishing the relationship between fast and slow memory

The experimental and modelling approaches we took were unable to resolve the branched and linear pathways. These assays are characterised by multiple timescales – the interdivision times and lifetimes of fast and slow subsets, the average waiting time to transition from fast to slow in the linear model, and the lifetime of Ki67 expression. We speculated that the rate of loss of Ki67 relative to the average rate of turnover of the population as a whole governed its utility for distinguishing the two models.

To explore this idea, we generated artificial BrdU/Ki67 labelling timecourses by simulating instances of the linear and branched models with added noise, and attempted to fit each model to data generated by the other. In one set of simulations, we used parameters similar to those derived from the fitting to the experimental data, in which fast cells had mean lifespans and interdivision times of a few days, comparable to the 3-4 day lifetime of Ki67 expression. In a second set of simulations, we separated the timescales by decreasing the duration of Ki67 expression to 3-4 hours, effectively making it a live readout of active cell division. In a third set, we artificially

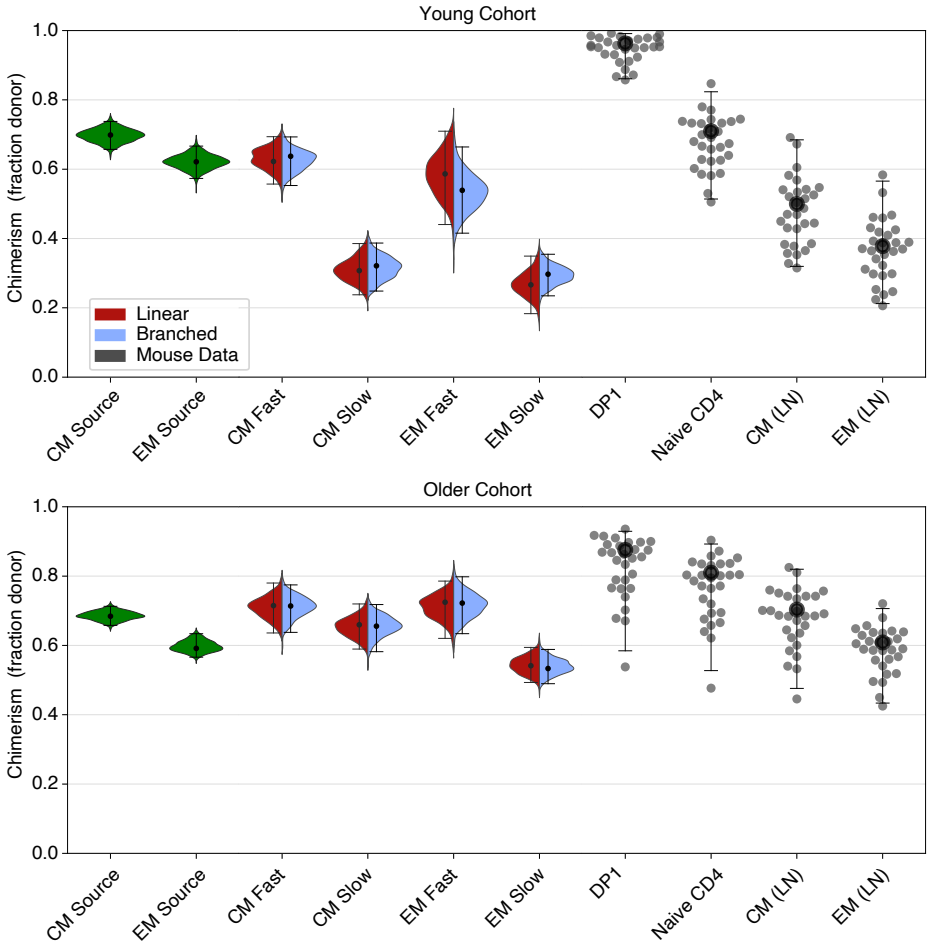

Figure 6 – Inferred and measured values of the chimerism (donor cell fraction) within thymic and peripheral T cell subpopulations. Left-hand (green) violin plots indicate the chimerism of the constitutive influxes into T_{CM} and T_{EM} estimated using Eq 1, f_d. Split-colour violin plots indicate the posterior distributions of the chimerism within fast and slow subsets of T_{CM} and T_{EM}; red and lilac indicate the linear and branched model predictions, respectively. Points represent experimentally observed donor fractions within early-stage double-positive thymocytes (DP1), naive T cells, and T_{CM} and T_{EM} derived from lymph nodes.

increased the lifespan of Ki67 to 10 days, such that it lay between the timescales of turnover of the fast and slow subsets.

Using the first set of simulations, we recapitulated our analyses of the experimental data; the branched and linear models were equally able to describe either dataset (using data generated by the linear model, ΔELPD with standard error was 1.8 (1.6); using data from branched model, 2.0 (2.0)). The ambiguity remained when we reduced the lifetime of Ki67. However, when its lifetime lay between that of fast and slow cells, we could distinguish the two pathways clearly (Fig S7; using data from linear model, linear model was superior, ΔELPD = 38 (10); using data from branched model, branched model was superior, ΔELPD = 8.5 (3.4)).

The reason for this result is unclear, but it may derive from the ability of our labelling system to distinguish fast and slow cells. Among CD4 T_{CM} and T_{EM}, the rates of self-renewal of fast and slow populations are so different that Ki67 expression can act as a proxy for fast/slow status. The utility of a marker of recent division as a proxy depends on its duration of expression, however. If it is very short, its frequency of expression will be low even among fast cells and so it becomes a poor (noisy) discriminant of fast and slow. If the marker's lifespan is very long, it becomes equivalent to BrdU as a label of division at any time in the past, and only distinguishes fast and slow cells very early in the assay, when uptake of BrdU is almost exclusively by fast cells. At intermediate lifespans, of the order the inverse of the mean lifespan of the population as a whole (see Eq 6), the absolute difference in Ki67 expression within fast and slow cells is maximal. We speculate that this reveals any transition of cells from fast to slow, which is the signature of the linear model.

Discussion

Our analysis shows that subtle shifts in the rates of turnover (loss) of memory CD4 T cells with their age can lead to quite large shifts in the population structure. We showed that the large differences in Ki67 expression between young and old memory populations was largely due to the fast/slow composition of each, rather than in any age-dependent changes in rates of self-renewal. Instead, we found that the longer memory clones persist, the lower their daily risk of loss. This kinetic will give rise to a long-tailed kinetic of memory clone survival. The mechanistic basis of these cell age effects are unclear. Memory T cells may undergo slow and heritable maturation that increases their expected time-to-die as they age. This might be a continuous process, or one that involves progression through discrete differentiation stages, such as the gradual acquisition of senescence markers. An alternative is a simple selection effect in which every cohort of new memory T cells is heterogeneous in its survival capacity, and more persistent clones are selected for over time.

The development and long-term maintenance of memory CD8 T cell subsets has been studied more extensively than that of CD4 T cells, and there are some key similarities with the results we describe here, as well as clues for resolving some of the ambiguities in our analyses. A study employing deuterium labelling of yellow fever virus (YFV)-specific CD8 T cells in humans [35] demonstrated a progressive shift to quiescence over months to years, with surviving memory T cells being very long lived and hardly dividing. Zarnitsyna *et al.* [36] explored a variety of mathematical models to quantify this slowing kinetic, and found strongest support for rates of both division and death that decline with time and generate a power-law decay in memory cell numbers. Akondy *et al.* [35] found that cells persisting long term were deuterium-rich, indicating that they were derived from populations that divided extensively in the days to weeks following challenge. This kinetic is consistent with a linear model of memory development from fast to slow, rather than the branched model we discussed more extensively here.

The identity and relationship of the fast and slow subsets within CD4 T_{CM} and T_{EM} remains unclear. MP CD4 T cells in bulk divide more rapidly on average than conventional antigen-specific memory cells [15–17]. Younes *et al.* [17] argued that MP CD4 T cells comprise a proliferative subset and a slower population with the properties of conventional memory. This distinction was motivated by the observation that bulk and LCMV-specific memory

CD4 T cells, identified with tetramer staining 15 days after LCMV challenge, were phenotypically similar, but had Ki67 expression levels of 25-40% and 5% respectively. Bulk memory is presumably enriched for MP cells, and indeed the frequencies of Ki67 expressing cells they observed among the tetramer-negative population are consistent with the roughly 30% weighted average among CD4 T_{CM} and T_{EM} in our analyses (Fig 2B). There have been conflicting reports regarding the signals required for the generation and maintenance of fast MP CD4 T cells. Younes *et al.* argued that they are driven by cytokines, based on the lack of an effect of an MHC class II-blocking antibody and a modest reduction in proliferation under IL-7R blockade [17]. Their results contrasted with reports that rapidly dividing MP CD4 T cells depend on interactions with MHC class II and require proximal TCR signalling kinases to sustain proliferation [16, 37], and have reduced dependence on IL-7 compared to antigen-specific CD4 memory [15]. However, later studies from the same lab as Younes *et al.* identified the importance of co-stimulation signals from CD28 for the proliferation of fast cells even though division was was not affected by MHC class II blockade [12]. The same study highlighted the importance of TCR and CD28 co-stimulation signals for the generation of MP CD4 T cells from naive precursors. One way of reconciling these various observations is if the generation and maintenance of MP CD4 T cells rely on CD28 and TCR interactions but vary in the threshold of TCR signalling required and if there is redundancy with CD28 signals. In addition, interpretation of MHC class II blockade experiments is heavily dependent upon whether antibody blockade is considered absolute, or, as is more likely the case, only partial. If the latter is true, the reduction in availability of MHC class II ligands may be sufficient to block priming events, but insufficient to halt self-renewal of existing memory.

Given the involvement of TCR signals in the production of new MP CD4 T cells, the difference in average levels of proliferation within bulk MP CD4 T cells and antigen-specific memory observed by Younes *et al.* [17] might be explained by the fact that MP T cells are continually produced in response to chronic and ubiquitous self or commensal stimuli, while LCMV-specific memory will become less proliferative with time post-challenge as the acute infection resolves and faster-dividing clones are progressively lost. One caveat is that the 4-fold disparity in Ki67 expression between tetramer-positive (LCMV-specific) and tetramer-negative (MP) CD4 T cells observed by Younes *et al.* [17] was manifest at 15 days post-challenge, indicating that in their system fast LCMV-specific memory persisted for only a few days, in contrast to the more extended residence times of fast populations, at the clonal level, that we inferred in our system. This difference suggests that the clonal lifespans of fast and slow MP T cells may be stimulus- or TCR-dependent. The binary characterisation of fast and slow that we model here may be a coarse-grained representation of a far more heterogeneous system in which T_{CM} and T_{EM} exhibit variability in their persistence times in a clone-specific way, perhaps depending on the antigenic burden they experience, or their T helper phenotype [38].

These results give further clues as to the sources of new CD4 T_{CM} and T_{EM}. By comparing the donor cell content of the constant flow of new cells entering the CD4 T_{CM} and T_{EM} pools to the donor fractions within other cell subsets, we saw clear evidence for a flux from T_{CM} to T_{EM}, likely from the rapidly dividing T_{CM} population. We also found evidence that newly produced T_{CM} derive largely from the naive CD4 T cell population in bulk. This was perhaps surprising; among mice housed in clean conditions, without overt infections, we expect naive T cells with appropriate TCR specificities for self or commensal antigens will be recruited into memory efficiently. In that case, one might expect recent thymic emigrants to be the dominant source of new memory, and so for this influx to be highly enriched for donor T cells. Instead, we saw substantial recruitment of host cells into memory long after bone marrow transplant, suggesting that even within SPF housing conditions, mice are regularly exposed to new antigenic stimuli. Alternatively, there may be a stochastic component to recruitment, such that naive T cells of any age have the potential to be stimulated to acquire a memory phenotype. Support for the latter idea comes from studies that implicate self antigens as important drivers of conversion to memory [12, 18], and that proliferation is greatest amongst $CD5^{hi}$ cells [12], a marker whose expression correlates with TCR avidity for self. Conversion to memory is therefore likely be an inefficient process since we would expect the naive precursors to be relatively low affinity for self-antigens; the majority of T cells with high affinity for self are deleted in the thymus. The efficiency of recruitment could also be subject to repression by regulatory T cells. Further,

within these relatively low affinity memory populations, any dependence of survival on affinity for self may explain the increase in the average clonal life expectancy over time. The preferential retention of such clones with age may be relevant to understanding the increasing incidence of autoimmune disease that occurs with old age. These ideas need to be tested in future studies.

Material and methods

Generation of busulfan chimeric mice

Busulfan chimeric C57Bl6/J mice were generated as described in ref. 23. In summary, WT CD45.1 and CD45.2 mice were bred and maintained in conventional pathogen-free colonies at the Royal Free Campus of University College London. CD45.1 mice aged 8 weeks were treated with 20 mg/kg busulfan (Busilvex, Pierre Fabre) to deplete HSC, and reconstituted with T-cell depleted bone marrow cells from congenic donor WT CD45.2 mice. Chimeras were sacrificed at weeks after bone marrow transplantation, and cells from the lymph nodes were analysed by flow cytometry. BrdU (Sigma) was administered to busulfan chimeric mice by an initial intraperitoneal injection of 0.8mg BrdU, followed by maintenance of 0.8mg/mL BrdU in drinking water for the indicated time periods up to 21 days. BrdU in drinking water was refreshed every 2-3 days. All experiments were performed in accordance with UK Home Office regulations, project license number PP2330953.

Flow cytometry

Cells were stained with the following monoclonal antibodies and cell dyes: CD45.1 FITC, CD45.2 AlexaFluor 700, TCR-beta APC, CD4 PerCP-eFluor710, CD25 PE, CD44 APC-eFluor780, CD25 eFluor450, CD62L eFluor450 (all eBioscience), TCR-beta PerCP-Cy5.5, CD5 BV510, CD4 BV650, CD44 BV785 (all BioLegend), CD62L BUV737 (BD Biosciences), LIVE/DEAD nearIR and LIVE/DEAD Blue viability dyes (Invitrogen). BrdU and Ki67 co-staining was performed using the FITC BrdU Flow Kit (BD Biosciences) according to the manufacturer's instructions, along with anti-Ki67 eFluor660 (eBioscience). Cells were acquired on a BD LSR-II or BD LSR-Fortessa flow cytometer and analysed using Flowjo software (Treestar). Subset gates were as follows: CD4 naive: live TCRb+ CD5+ CD4+ CD25- CD44- CD62L+. T_{EM}: live TCRb+ CD5+ CD4+ CD25- CD44+ CD62L-. T_{CM}: live TCRb+ CD5+ CD4+ CD25- CD44+ CD62L+.

Mathematical modelling and statistical analysis

All mathematical models are detailed in S1 Text and our approach to model fitting is details in S2 Text. Code and data used to perform model fitting, and details of the prior distributions for parameters, are available at `github.com/elisebullock/tcellmemorypaper`. Models were ranked using the Leave-One-Out (LOO) cross validation method [39]. We quantified the relative support for models with the expected log pointwise predictive density (ELPD), for which we reported the standard error. Models with ELPD differences below 4 were considered similar.

Supporting Tables

Population	Cohort	Daily influx (MAP and 95% CI) - cells per day	
		Donor	Host
CD4 T_{CM}	Young	1400 (1200, 1700)	610 (490, 740)
	Old	1400 (1200, 1600)	630 (520, 750)
CD4 T_{EM}	Young	14000 (12000, 16000)	8200 (6900, 9800)
	Old	13000 (11000, 15000)	9200 (7500, 11000)

Table S1 – MAP estimates and 95% credible intervals on the total daily rate of influx of cells into the CD4 T_{CM} and T_{EM} pools, relative to (Eq. 1 and Fig S2).

Parameter	Population	Cohort	Estimate (MAP and 95% CI)		
			Donor	Host	Difference
Fraction of influx entering fast subset	CM	Young	0.76 (0.52, 0.9)	0.61 (0.39, 0.88)	0.057 (-0.21, 0.38)
	CM	Old	0.55 (0.37, 0.8)	0.57 (0.34, 0.8)	0.028 (-0.32, 0.32)
	EM	Young	0.24 (0.15, 0.45)	0.24 (0.14, 0.53)	0.013 (-0.3, 0.23)
	EM	Old	0.31 (0.21, 0.56)	0.42 (0.28, 0.72)	-0.13 (-0.38, 0.17)
Mean interdivision time (Fast) (days)	CM	Young	4.8 (4.2, 5.4)	4.1 (3.5, 4.8)	0.64 (-0.19, 1.4)
	CM	Old	4.1 (3.6, 4.5)	3.8 (3.3, 4.4)	0.42 (-0.53, 0.99)
	EM	Young	7.5 (6.3, 8.7)	7.5 (5.9, 9.3)	0.26 (-2.3, 2.2)
	EM	Old	6.6 (5.6, 7.6)	6.2 (4.8, 8.4)	0.58 (-2, 2.2)
Mean lifetime (Fast) (days)	CM	Young	4.5 (4, 5)	3.9 (3.4, 4.5)	0.51 (-0.26, 1.2)
	CM	Old	3.8 (3.4, 4.3)	3.5 (3, 4.2)	0.43 (-0.51, 0.96)
	EM	Young	6.8 (5.9, 7.9)	6.7 (5.3, 8.6)	0.2 (-2, 1.9)
	EM	Old	5.8 (4.9, 6.7)	4.9 (3.7, 5.9)	1.1 (-0.37, 2.6)
Mean interdivision time (Slow) (days)	CM	Young	180 (98, 750)	190 (130, 510)	3.4 (-220, 560)
	CM	Old	140 (93, 360)	150 (110, 450)	-6.4 (-280, 190)
	EM	Young	340 (190, 900)	160 (110, 460)	200 (-100, 750)
	EM	Old	130 (93, 330)	140 (110, 360)	-12 (-170, 170)
Mean lifetime (Slow) (days)	CM	Young	56 (43, 95)	120 (98, 160)	-56 (-99, -20)
	CM	Old	61 (55, 73)	71 (62, 87)	-9.1 (-26, 5.1)
	EM	Young	40 (36, 50)	72 (62, 86)	-29 (-45, -18)
	EM	Old	47 (42, 55)	57 (52, 68)	-10 (-21, -1.4)
Efficiency of BrdU uptake per division	CM	Young	0.53 (0.51, 0.57)	0.54 (0.52, 0.58)	-0.011 (-0.053, 0.039)
	CM	Old	0.66 (0.63, 0.7)	0.66 (0.61, 0.71)	-0.0027 (-0.063, 0.064)
	EM	Young	0.56 (0.51, 0.6)	0.57 (0.52, 0.62)	-0.0047 (-0.077, 0.064)
	EM	Old	0.73 (0.68, 0.78)	0.69 (0.64, 0.77)	0.043 (-0.055, 0.12)
Rate of loss of BrdU in source during delabelling	CM	Young	0.18 (0.15, 0.21)	0.17 (0.15, 0.2)	0.0059 (-0.032, 0.04)
	CM	Old	0.18 (0.15, 0.2)	0.17 (0.15, 0.2)	0.0038 (-0.036, 0.041)
	EM	Young	0.19 (0.16, 0.22)	0.18 (0.15, 0.21)	-0.0018 (-0.042, 0.049)
	EM	Old	0.19 (0.16, 0.22)	0.18 (0.16, 0.22)	-0.0014 (-0.043, 0.046)
Ki67 lifetime (days)	CM	Young	3.1 (3.1, 3.2)	3.1 (3.1, 3.2)	0.0041 (-0.07, 0.074)
	CM	Old	3.2 (3.1, 3.3)	3.2 (3.1, 3.4)	-0.0062 (-0.21, 0.12)
	EM	Young	3.1 (3.1, 3.2)	3.1 (3.1, 3.2)	0.0005 (-0.068, 0.057)
	EM	Old	3.1 (3.1, 3.2)	3.2 (3.1, 3.3)	-0.021 (-0.15, 0.056)
Proportion Fast	CM	Young	0.69 (0.65, 0.75)	0.39 (0.35, 0.42)	0.31 (0.24, 0.37)
	CM	Old	0.44 (0.4, 0.47)	0.37 (0.34, 0.41)	0.062 (0.0082, 0.11)
	EM	Young	0.43 (0.38, 0.49)	0.21 (0.16, 0.28)	0.21 (0.13, 0.29)
	EM	Old	0.3 (0.25, 0.34)	0.16 (0.13, 0.2)	0.13 (0.076, 0.19)
Net loss rate of fast cells (λ_A)	CM	Young	0.014 (0.0096, 0.018)	0.0092 (0.0053, 0.015)	0.0042 (-0.0017, 0.01)
	CM	Old	0.014 (0.0099, 0.025)	0.016 (0.009, 0.028)	-0.00091 (-0.013, 0.011)
	EM	Young	0.0095 (0.0059, 0.019)	0.011 (0.0051, 0.025)	0.00072 (-0.016, 0.0097)
	EM	Old	0.016 (0.011, 0.032)	0.054 (0.028, 0.093)	-0.031 (-0.072, -0.0044)
Net loss rate of slow cells (λ_B)	CM	Young	0.012 (0.0048, 0.019)	0.0031 (0.0011, 0.006)	0.0091 (0.0012, 0.016)
	CM	Old	0.01 (0.0045, 0.014)	0.0087 (0.0035, 0.012)	0.0025 (-0.0052, 0.0082)
	EM	Young	0.021 (0.017, 0.026)	0.0076 (0.005, 0.011)	0.013 (0.0083, 0.018)
	EM	Old	0.015 (0.0092, 0.019)	0.012 (0.0061, 0.015)	0.003 (-0.0033, 0.01)
Ratio of fast:slow loss rates (λ_A/λ_B)	CM	Young	0.97 (0.53, 3.4)	2.2 (1, 12)	-1.1 (-11, 1.2)
	CM	Old	1.5 (0.78, 5.1)	2 (0.84, 7)	-0.33 (-5.3, 3.5)
	EM	Young	0.41 (0.26, 1)	1.2 (0.53, 4.8)	-0.66 (-3.9, 0.18)
	EM	Old	1.1 (0.65, 3.3)	4.2 (1.9, 15)	-2.7 (-13, 0.14)
Proportion Ki67^{high}	CM	Young	0.53 (0.51, 0.54)	0.32 (0.31, 0.34)	0.2 (0.18, 0.23)
	CM	Old	0.38 (0.36, 0.39)	0.34 (0.32, 0.35)	0.039 (0.017, 0.062)
	EM	Young	0.29 (0.27, 0.31)	0.17 (0.16, 0.18)	0.12 (0.1, 0.14)
	EM	Old	0.24 (0.23, 0.25)	0.17 (0.16, 0.18)	0.073 (0.06, 0.089)

Table S2 – MAP estimates and 95% credible intervals on parameters estimated using the branched model.

Supporting Figures

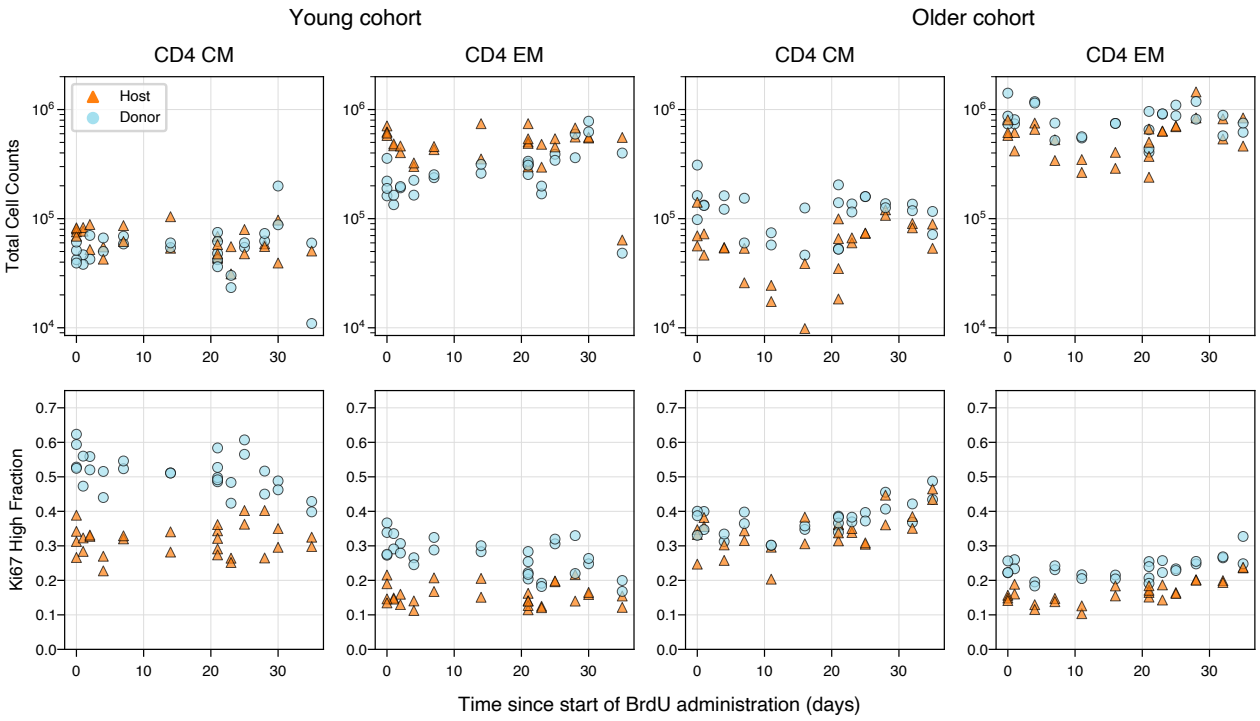

Figure S1 – Numbers and Ki67 expression of both host and donor CD4 T_{CM} and T_{EM} over the timecourses of the labelling experiments in young and older cohorts of busulfan chimeras.

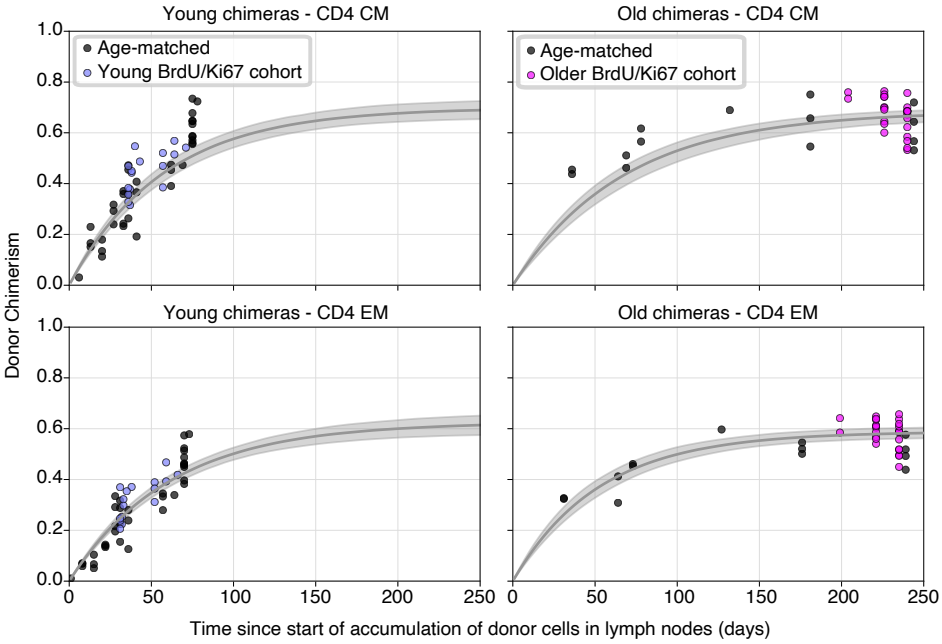

Figure S2 – Estimating the influx into the CD4 T_{CM} and T_{EM} pools in young and old mice. Curves are the fitted trajectories of $D(t)/N$, from the solution to Eq 1. Black points represent data from age-matched busulfan chimeric mice from other experiments. Envelopes are derived from sampling the 95% credible intervals of the parameters.

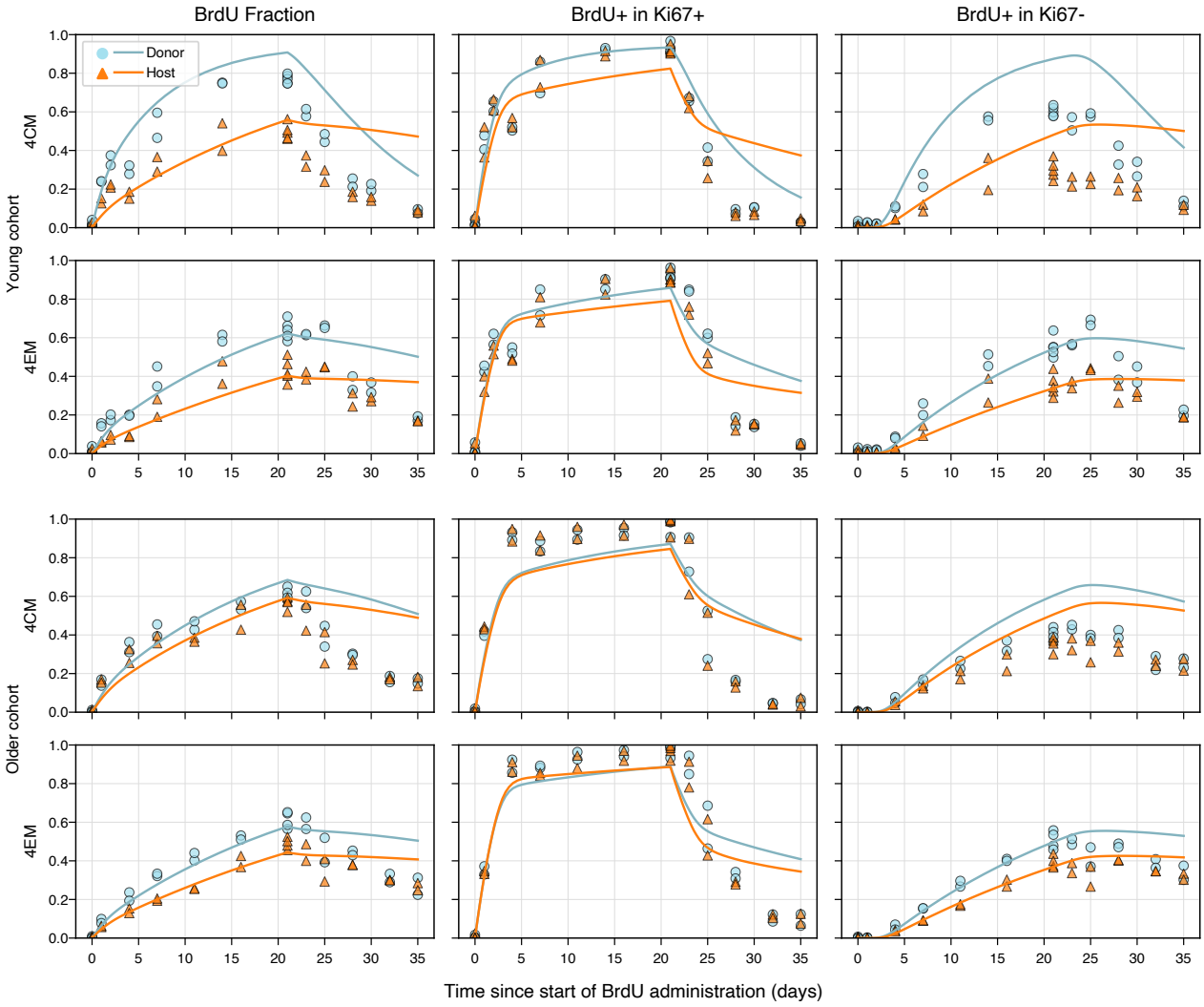

Figure S3 – Fits of the temporal heterogeneity model to the BrdU/Ki67 labelling data.

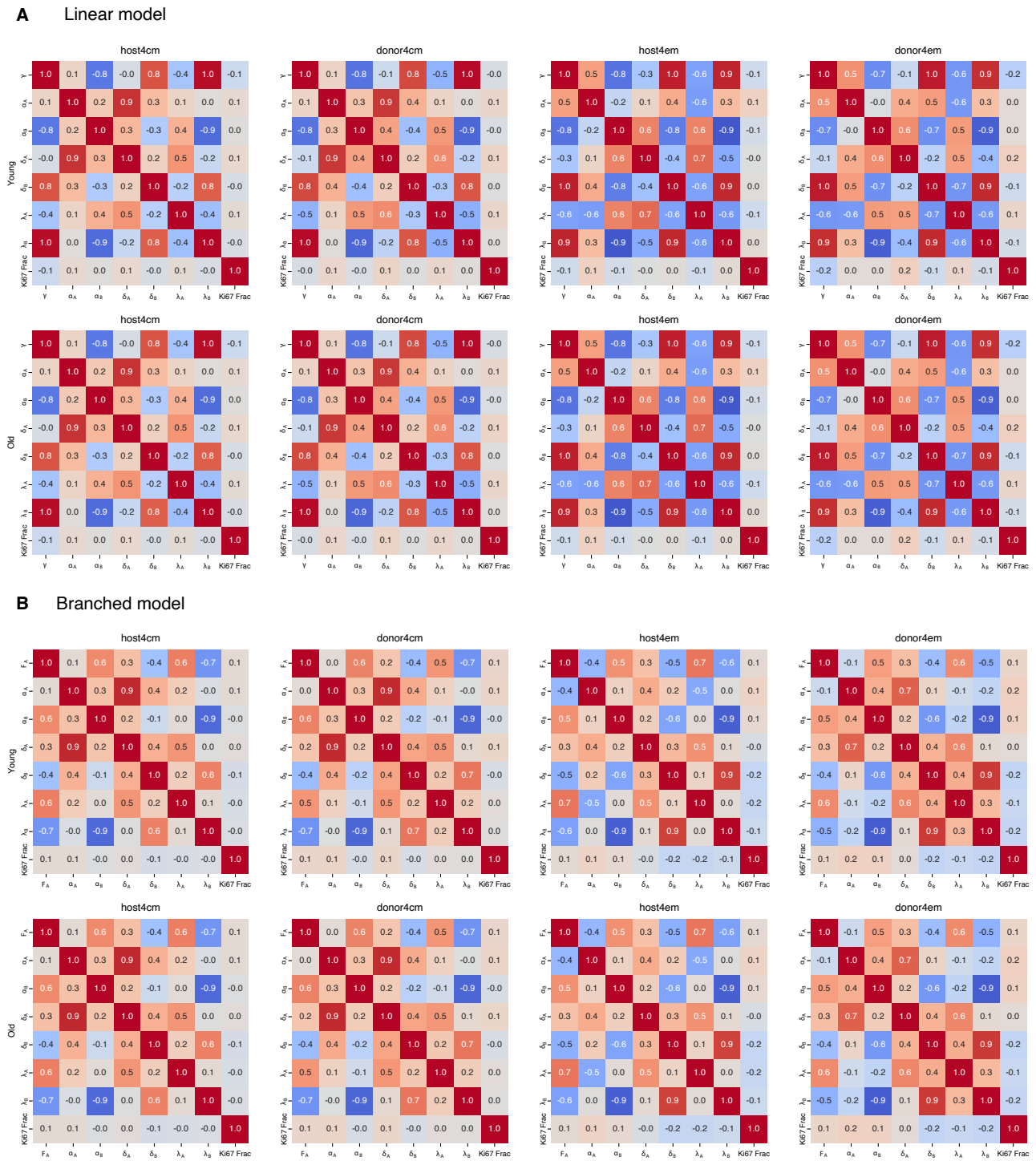

Figure S4 – Correlations in parameters observed in fits of (A) the linear model, and (B) the branched model.

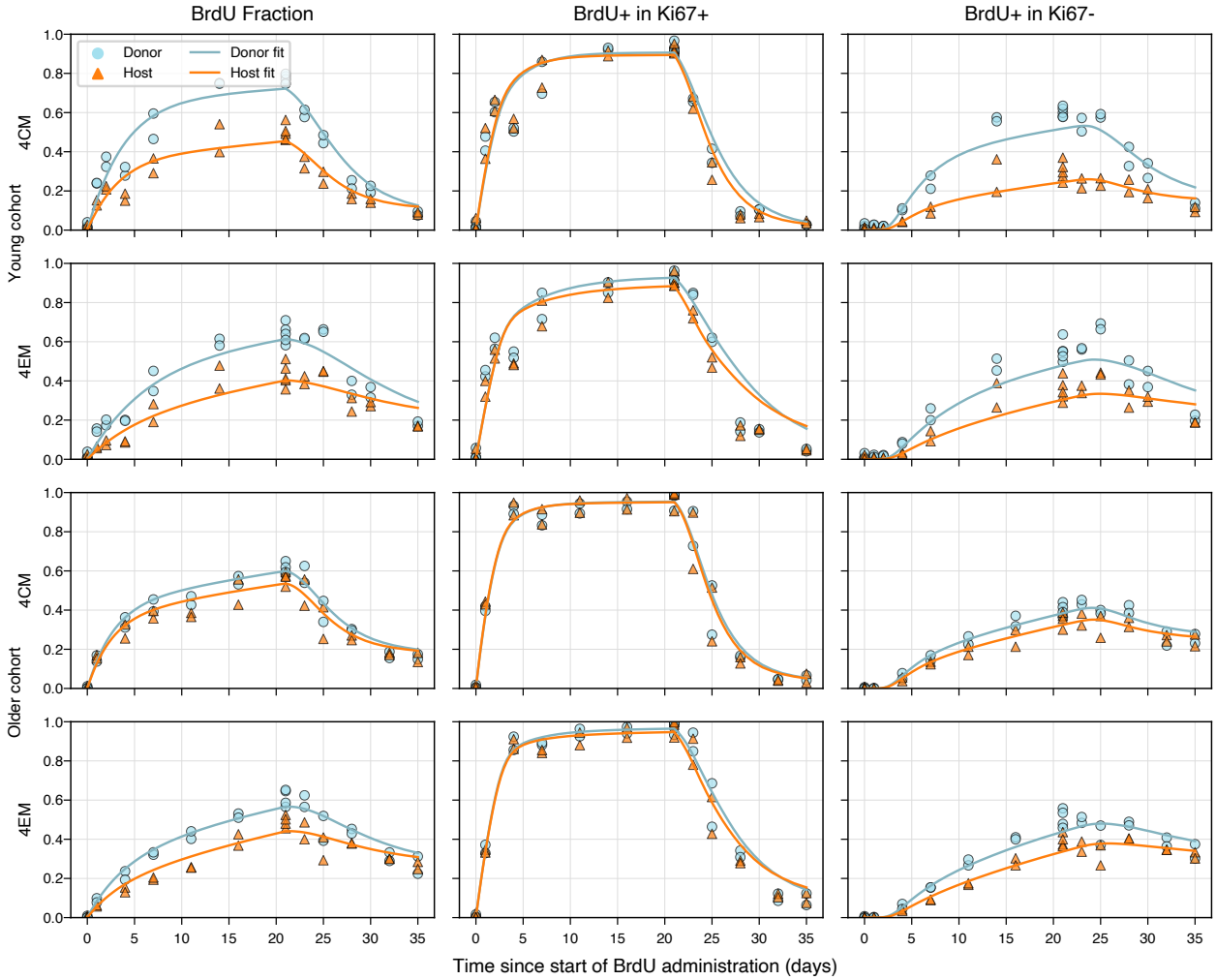

Figure S5 – Fits of the linear model to the BrdU/Ki67 labelling data.

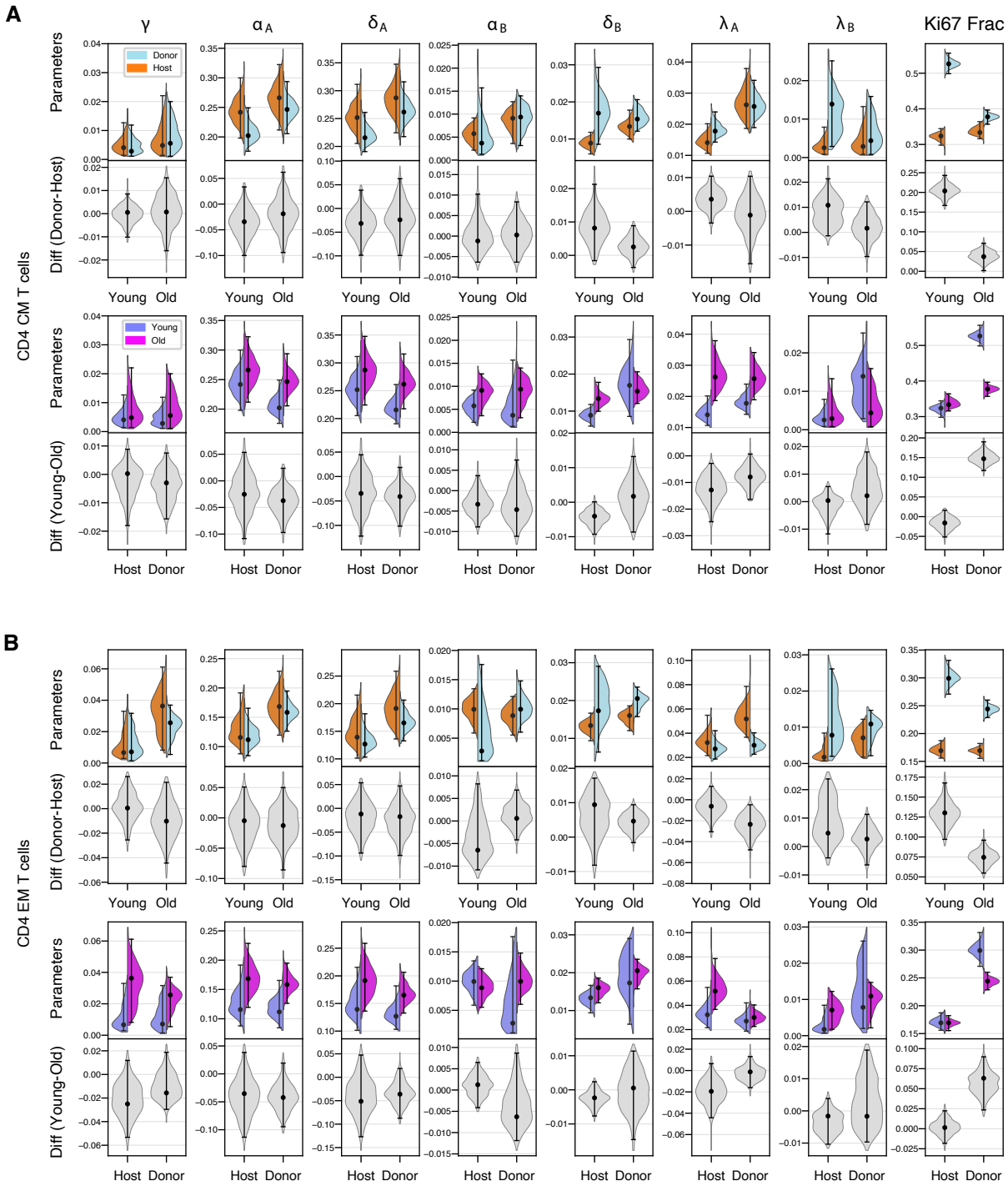

Figure S6 – Parameter estimates for the linear model, for CD4 T_{CM} (**A**) and CD4 T_{EM} (**B**).

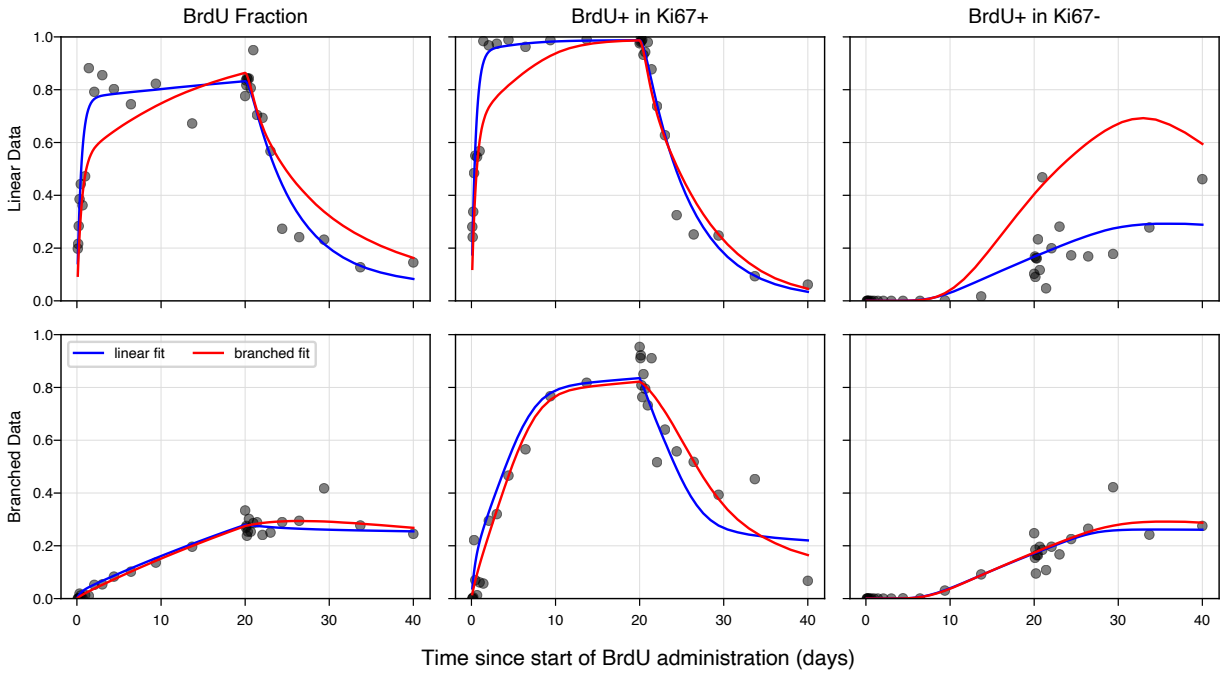

Figure S7 – Fitting the linear and branched models to artificial data generated by the linear model (upper panels) and the branched model (lower panels).

S1 Text Mathematical modelling

Modelling BrdU/Ki67 pulse-chase labelling. We used ordinary differential equation models to describe the fluxes of cells between the BrdU$^{+/-}$ Ki67$^{\text{high/low}}$ populations within the CD4 T_{CM} and T_{EM} subsets. Prior distributions on the rates of flow of new cells into each subset (θ) were chosen to be the posterior distributions on θ obtained from modelling the accumulation of donor cells in busulfan chimeric mice, as described in the main text. We assumed that kinetic heterogeneity within each subset could be represented with two subpopulations with distinct rates of division and death. In the branched model, these subpopulations (denoted A and B) are fed separately from the same precursor, at total rate θ, in unknown proportions. The linear model assumes constant flow from source into population A, which then transitions into population B at per capita rate γ. In both models, cells from from the precursor population are assumed to be Ki67^{high}, based on the assumption that new memory T cells have recently undergone clonal expansion.

Levels of Ki67 protein decay smoothly after mitosis, but in our flow cytometry analysis, cells are categorized into binary states Ki67^{high} and Ki67^{low}. We therefore modeled the transition between these two states with intermediate Ki67^{high} compartments, such that the residence time within the Ki67^{high} compartment is gamma distributed. During the labelling phase, the delay before BrdU+Ki67^{low} cells appeared was clearly apparent, suggesting that the variance in the residence time within Ki67^{high} was small. Therefore used 10 intermediate Ki67^{high} states. We also used two intermediate BrdU compartments, reflecting the assumption that in the absence of label, BrdU-positive cells become BrdU-negative after two divisions.

The following equations describe the BrdU labelling and de-labelling phases for both models. For the branched model, the parameter F_A denotes the fraction of the influx that enters subset A, while γ (the rate at which type A cells differentiate into type B) was set to zero. For the linear model, γ was a free parameter, while F_A was set to one.

Labelling phase:

$$\frac{d}{dt}A^{\hat{b}}_{\hat{k}} = F_A\theta - (\delta_A + \gamma + \hat{k}\beta + \alpha_A)A^{\hat{b}}_{\hat{k}} + 2\epsilon\alpha_A\sum_{i=0}^{\hat{b}}\sum_{j=0}^{\hat{k}} A^i_j$$

$$\frac{d}{dt}A^i_{\hat{k}} = 2(1-\epsilon)\alpha_A\sum_{j=0}^{\hat{k}} A^{i+1}_j - (\delta_A + \gamma + \alpha_A + \hat{k}\beta)A^i_{\hat{k}} \qquad \text{for } 1 \le i < \hat{b}$$

$$\frac{d}{dt}A^0_{\hat{k}} = 2(1-\epsilon)\alpha_A\sum_{i=0}^{1}\sum_{j=0}^{\hat{k}} A^i_j - (\delta_A + \gamma + \alpha_A + \hat{k}\beta)A^0_{\hat{k}}$$

$$\frac{d}{dt}A^i_j = \hat{k}\beta A^i_{j+1} - (\delta_A + \gamma + \alpha_A + \hat{k}\beta)A^i_j \qquad \text{for } 0 \le i \le \hat{b} \text{ and and } 1 \le j < \hat{k}$$

$$\frac{d}{dt}A^i_0 = \hat{k}\beta A^i_1 - (\delta_A + \gamma + \alpha_A)A^i_0 \qquad \text{for } 0 \le i \le \hat{b}$$

$$\frac{d}{dt}B^{\hat{b}}_{\hat{k}} = (1-F_A)\theta + \gamma A^{\hat{b}}_{\hat{k}} - (\delta_B + \hat{k}\beta + \alpha_B)B^{\hat{b}}_{\hat{k}} + 2\epsilon\alpha_B\sum_{i=0}^{\hat{b}}\sum_{j=0}^{\hat{k}} B^i_j$$

$$\frac{d}{dt}B^i_{\hat{k}} = \gamma A^i_{\hat{k}} + 2(1-\epsilon)\alpha_B\sum_{j=0}^{\hat{k}} B^{i+1}_j - (\delta_B + \alpha_B + \hat{k}\beta)B^i_{\hat{k}} \qquad \text{for } 1 \le i < \hat{b}$$

$$\frac{d}{dt}B^0_{\hat{k}} = \gamma A^0_{\hat{k}} + 2(1-\epsilon)\alpha_B\sum_{i=0}^{1}\sum_{j=0}^{\hat{k}} B^i_j - (\delta_B + \alpha_B + \hat{k}\beta)B^0_{\hat{k}}$$

$$\frac{d}{dt}B^i_j = \gamma A^i_j + \hat{k}\beta B^i_{j+1} - (\delta_B + \alpha_B + \hat{k}\beta)B^i_j \qquad \text{for } 0 \le i \le \hat{b} \text{ and } 1 \le j < \hat{k}$$

$$\frac{d}{dt}B^i_0 = \gamma A^i_0 + \hat{k}\beta B^i_1 - (\delta_B + \alpha_B)B^i_0 \qquad \text{for } 0 \le i \le \hat{b}$$

De-labelling phase:

$$\frac{d}{dt}A^{\hat{b}}_{\hat{k}} = F_A\theta e^{-\mu t} - (\delta_A + \gamma + \hat{k}\beta + \alpha_A)A^{\hat{b}}_{\hat{k}}$$

$$\frac{d}{dt}A^i_{\hat{k}} = 2\alpha_A\sum_{j=0}^{\hat{k}} A^{i+1}_j - (\delta_A + \gamma + \alpha_A + \hat{k}\beta)A^i_{\hat{k}} \qquad \text{for } 1 \le i < \hat{b}$$

$$\frac{d}{dt}A^0_{\hat{k}} = F_A\theta(1-e^{-\mu t}) + 2\alpha_A\sum_{i=0}^{1}\sum_{j=0}^{\hat{k}} A^i_j - (\delta_A + \gamma + \alpha_A + \hat{k}\beta)A^0_{\hat{k}}$$

$$\frac{d}{dt}A^i_j = \hat{k}\beta A^i_{j+1} - (\delta_A + \gamma + \alpha_A + \hat{k}\beta)A^i_j \qquad \text{for } 0 \le i \le \hat{b} \text{ and } 1 \le j < \hat{k}$$

$$\frac{d}{dt}A^i_0 = \hat{k}\beta A^i_1 - (\delta_A + \gamma + \alpha_A)A^i_0 \qquad \text{for } 0 \le i \le \hat{b}$$

$$\frac{d}{dt}B^{\hat{b}}_{\hat{k}} = (1-F_A)\theta e^{-\mu t} + \gamma A^{\hat{b}}_{\hat{k}} - (\delta_B + \hat{k}\beta + \alpha_B)B^{\hat{b}}_{\hat{k}}$$

$$\frac{d}{dt}B^i_{\hat{k}} = \gamma A^i_{\hat{k}} + 2\alpha_B\sum_{j=0}^{\hat{k}} B^{i+1}_j - (\delta_B + \alpha_B + \hat{k}\beta)B^i_{\hat{k}} \qquad \text{for } 1 \le i < \hat{b}$$

$$\frac{d}{dt}B^0_{\hat{k}} = (1-F_A)\theta(1-e^{-\mu t}) + \gamma A^0_{\hat{k}} - (\delta_B + \alpha_B + \hat{k}\beta)B^0_{\hat{k}} + +2\alpha_B\sum_{i=0}^{1}\sum_{j=0}^{\hat{k}} B^i_j$$

$$\frac{d}{dt}B^i_j = \gamma A^i_j + \hat{k}\beta B^i_{j+1} - (\delta_B + \alpha_B + \hat{k}\beta)B^i_j \qquad \text{for } 0 \le i \le \hat{b} \text{ and } 1 \le j < \hat{k}$$

$$\frac{d}{dt}B^i_0 = \gamma A^i_0 + \hat{k}\beta B^i_1 - (\delta_B + \alpha_B)B^i_0 \qquad \text{for } 0 \le i \le \hat{b}$$

S2 Text Model fitting

Initialization Motivated by the experimental observations that cells numbers and Ki67 expression levels were approximately constant over the labelling assay, we assumed that each memory population (T_{CM} and T_{EM}, host/donor) was in (quasi-) equilibrium. To establish initial conditions for the model for each sampled set of parameters, we set all BrdU-labelled species to zero, and used the bk45 ODE solver to 10000 days to allow the system to attain steady state. This provided the initial sizes of all species prior to BrdU administration.

Modelling noise/mouse-to-mouse variation The model yields total cell numbers and the proportions of cells in the four quadrants of BrdU$^{\pm}$ Ki67$^{\pm}$. We assumed that uncertainty in the total numbers was lognormally distributed, and used a Dirichlet multinomial model to describe the assignment of cells to each of the four quadrants. The Dirichlet multinomial distribution is a continuous, multivariate distribution for k variables $x_1 \dots x_k$ where each $x_i \in (0,1)$ and $\Sigma_{i=1}^{k} x_i = 1$. Uncertainty in the assignment of cells to quadrants – which principally reflects variation between mice in the frequencies of cells in each quadrant – was described with an overdispersion parameter ϕ with an exponential prior.

Definition of priors For consistency of interpretation, we defined the subsets' loss rates (δ_A and δ_B) and division rates (α_A and α_B) such that the rates defining subset A were greater than those defining B. In addition each loss rate δ was constrained to be greater than the division rate to ensure the population remained at steady state with an influx of cells. The Ki67 lifetime $1/\beta$ was constrained to lie within 3-4 days, based on our previous studies. We chose broad priors for the rate of loss of BrdU within the source (μ) in the delabelling phase, and the efficiency of BrdU uptake per cell division during the labelling phase (ϵ). Details of priors are given at `github.com/elisebullock/tcellmemorypaper`.

S3 Text Estimating influx

Within busulfan chimeric mice, this accumulation of donor-derived T_{CM} or T_{EM} (Fig S2) was well described by a simple model with a single average rate of turnover, λ;

$$\text{Donor cells} \quad \frac{dD}{dt} = f_d\theta - \lambda D; \qquad \text{Host cells} \quad \frac{dH}{dt} = (1-f_d)\theta - \lambda H, \tag{1}$$

where f_d is the proportion of the constitutive influx of memory θ that comprises donor cells, and we model from the time at which donor memory T cells start to appear in lymph nodes. For each subset (T_{CM} and T_{EM}) and in young and old mice, we fitted this model simultaneously to the steady state numbers $N = D + H = \theta/\lambda$ and the chimerism timecourse $D(t)/N$ (Fig S2), using data from the chimeric mice we studied here augmented with data from age-matched chimeric mice aggregated from other experiments. This procedure yielded posterior distributions of the total (host plus donor) influx rates θ (Table S1) that were only weakly correlated with those of the other parameters (N, λ, and f_d).

S4 Text Calculation of mean lifespan in the branched model

Suppose the donor fraction is f_D, the fast cell fractions within host and donor are f_A^H and f_A^D, respectively, and δ_A^D and δ_B^D are the loss rates of fast and slow donor cells, respectively, with correspondingly δ_A^H and δ_B^H for host cells. Then the population-average loss rate $\bar{\delta}$ is given by

$$\begin{aligned} \bar{\delta} &= f_D\bar{\delta}_D + (1-f_D)\bar{\delta}_H, \\ \text{where } \bar{\delta}_D &= f_A^D\delta_A^D + (1-f_A^D)\delta_B^D \text{ and } \bar{\delta}_H = f_A^H\delta_A^H + (1-f_A^H)\delta_B^H. \end{aligned}$$

The mean lifespan is then $1/\bar{\delta}$.

S5 Text Obtaining mean lifespans through estimating the total production rate

We present two methods of obtaining an approximate average loss rate (and hence mean lifespan) by measuring the total rate of production. These are equal for a population at equilibrium.

The first is to use information contained in the initial growth in the BrdU labelled fraction. De Boer and Perelson [33] used data from Younes *et al.* [17] who found that 35% and 60% of memory CD4 T cells were BrdU$^+$ after 3 and 10 days of labelling, respectively, to estimate an expected life span of between 14 and 22 days. To generalise their modelling approach, consider a memory population of size N at equilibrium, fed from a source at rate θ, dividing at average rate α, and lost at rate δ. During BrdU administration, assume the source is entirely labelled, and unlabelled memory cells take up BrdU with probability ϵ per division. If we denote unlabelled cells N_U and labelled cells N_L, then

$$\frac{dN_U}{dt} = -(\epsilon\alpha + \delta)N_U + (1-\epsilon)\alpha N_U, \quad \frac{dN_L}{dt} = \theta + 2\epsilon\alpha N_U + (\alpha - \delta)N_L. \tag{2}$$

The labelled fraction $L = N_L/N$ is given by

$$\frac{dL}{dt} = \frac{1}{N}\frac{dN_L}{dt} = (\delta - \alpha + 2\epsilon\alpha)(1-L), \tag{3}$$

where we have used $N_U = N - N_L$, and the steady state condition $dN/dt = 0$ yielding $\theta/N = \delta - \alpha$. The initial upslope of the labelled fraction L is then $p = \delta - \alpha + 2\epsilon\alpha$. If the source is entirely unlabelled,

$$\frac{dL}{dt} = 2\epsilon\alpha - L(2\epsilon\alpha - \alpha + \delta), \tag{4}$$

and so $p = 2\epsilon\alpha$. Therefore, depending on the rate of influx and its label content, the initial upslope in the BrdU$^+$ fraction can be a combination of both the average division and loss rates, as well as the uptake efficiency.

De Boer and Perelson's calculation assumed that memory CD4 T cells are entirely self-renewing, such that $\theta = 0$ and $\alpha = \delta$, and that uptake of BrdU by dividing cells is 100% efficient. Eq 4 then yields $dL/dt = 2\delta(1-L)$, which they fitted to the Younes data to obtain the average lifespan $1/\delta$. The self-renewing approximation is reasonable – we estimate that the influxes into T_{CM} and T_{EM} are of the order 1% of the population size per day, so we can proceed by neglecting them. However we established that the BrdU uptake efficiency ϵ is considerably less than 1, and was well constrained by the steepness of growth in the BrdU$^+$Ki67^{high} fraction ($\epsilon = 0.55$ in younger cohort, and 0.75 in the older cohort, which were separate experiments). The mean lifespan is then reduced to $2\epsilon/p$, as quoted in the main text.

The second approach is to derive an average rate of turnover using the frequency of cells expressing Ki67. Consider again the memory population at steady state size N with cells entering at rate θ, dividing at an average rate α and dying at average rate δ:

$$\frac{dN}{dt} = \theta + (\alpha - \delta)N = 0 \implies \alpha N + \theta = \delta N. \tag{5}$$

Suppose Ki67 is expressed for a time T after cell division, and that all cells entering memory are Ki67^{high}. Then the number of cells in the population at any time t that are Ki67^{high}, K^+, is equal to the number that entered or divided in the last T days, and survived to time t:

$$K^+ = \int_{t-T}^{t} (\alpha N + \theta)\, e^{-\delta(s-T)} ds = \frac{\alpha N + \theta}{\delta}(1 - e^{-\delta T}). \tag{6}$$

Using Eq 5, the Ki67^{high} proportion $k = K^+/N = 1 - e^{-\delta T}$. The mean lifespan $\tau = 1/\delta$ is then

$$\tau = \frac{-T}{\ln(1-k)}. \tag{7}$$

References

1. Swain SL, Agrewala JN, Brown DM, Jelley-Gibbs DM, Golech S, Huston G, et al. CD4+ T-cell memory: generation and multi-faceted roles for CD4+ T cells in protective immunity to influenza. Immunological reviews. 2006;211(1):8–22.
2. Tubo NJ, Jenkins MK. CD4+ T Cells: guardians of the phagosome. Clin Microbiol Rev. 2014;27(2):200–13. doi:10.1128/CMR.00097-13.
3. Künzli M, Masopust D. CD4+ T cell memory. Nature Immunology. 2023;16:4. doi:10.1038/s41590-023-01510-4.
4. Westera L, Drylewicz J, den Braber I, Mugwagwa T, van der Maas I, Kwast L, et al. Closing the gap between T-cell life span estimates from stable isotope-labeling studies in mice and humans. Blood. 2013;122(13):2205–12. doi:10.1182/blood-2013-03-488411.
5. Gossel G, Hogan T, Cownden D, Seddon B, Yates AJ. Memory CD4 T cell subsets are kinetically heterogeneous and replenished from naive T cells at high levels. eLife. 2017;6:e23013. doi:10.7554/eLife.23013.
6. Baliu-Piqué M, Verheij MW, Drylewicz J, Ravesloot L, de Boer RJ, Koets A, et al. Short Lifespans of Memory T-cells in Bone Marrow, Blood, and Lymph Nodes Suggest That T-cell Memory Is Maintained by Continuous Self-Renewal of Recirculating Cells. Front Immunol. 2018;9:2054.
7. Borghans JAM, Tesselaar K, de Boer RJ. Current best estimates for the average lifespans of mouse and human leukocytes: reviewing two decades of deuterium-labeling experiments. Immunol Rev. 2018;285(1):233–248.
8. Baliu-Piqué M, Otto SA, Borghans JAM, Tesselaar K. In vivo deuterium labelling in mice supports a dynamic model for memory T-cell maintenance in the bone marrow. Immunol Lett. 2019;210:29–32.
9. Derksen LY, Tesselaar K, Borghans JAM. Memories that last: Dynamics of memory T cells throughout the body. Immunol Rev. 2023;316(1):38–51. doi:10.1111/imr.13211.
10. del Amo PC, Beneytez JL, Boelen L, Ahmed R, Miners KL, Zhang Y, et al. Human TSCM cell dynamics in vivo are compatible with long-lived immunological memory and stemness. PLoS Biology. 2018;16(6):1–22.
11. Jameson SC, Lee YJ, Hogquist KA. Innate Memory T cells. In: Advances in Immunology. vol. 126. Adv Immunol; 2015. p. 173–213.
12. Kawabe T, Jankovic D, Kawabe S, Huang Y, Lee PHH, Yamane H, et al. Memory-phenotype CD4+ T cells spontaneously generated under steady state conditions exert innate Th1-like effector function. Science Immunology. 2017;2(12):16.
13. Min B, Paul WE. Endogenous proliferation: burst-like CD4 T cell proliferation in lymphopenic settings. Semin Immunol. 2005;17(3):201–7. doi:10.1016/j.smim.2005.02.005.
14. Tough DF, Sprent J. Turnover of naive- and memory-phenotype T cells. J Exp Med. 1994;179(4):1127–35.
15. Lenz DC, Kurz SK, Lemmens E, Schoenberger SP, Sprent J, Oldstone MB, et al. IL-7 regulates basal homeostatic proliferation of antiviral CD4+T cell memory. Proc Natl Acad Sci U S A. 2004;101(25):9357–62.
16. Purton JF, Tan JT, Rubinstein MP, Kim DM, Sprent J, Surh CD. Antiviral CD4+ memory T cells are IL-15 dependent. J Exp Med. 2007;204(4):951–61.
17. Younes SA, Punkosdy G, Caucheteux S, Chen T, Grossman Z, Paul WE. Memory phenotype CD4 T cells undergoing rapid, nonburst-like, cytokine-driven proliferation can be distinguished from antigen-experienced memory cells. PLoS Biology. 2011;9(10):e1001171.

18. Hogan T, Nowicka M, Cownden D, Pearson CF, Yates AJ, Seddon B. Differential impact of self and environmental antigens on the ontogeny and maintenance of CD4+ T cell memory. eLife. 2019;8. doi:10.7554/eLife.48901.

19. Mohri H, Perelson AS, Tung K, Ribeiro RM, Ramratnam B, Markowitz M, et al. Increased turnover of T lymphocytes in HIV-1 infection and its reduction by antiretroviral therapy. J Exp Med. 2001;194(9):1277–87.

20. Asquith B, Debacq C, Macallan DC, Willems L, Bangham CRM. Lymphocyte kinetics: the interpretation of labelling data. Trends in Immunology. 2002;23(12):596–601.

21. Ganusov VV, Borghans JAM, De Boer RJ. Explicit kinetic heterogeneity: mathematical models for interpretation of deuterium labeling of heterogeneous cell populations. PLoS Comput Biol. 2010;6(2):e1000666.

22. Hogan T, Gossel G, Yates AJ, Seddon B. Temporal fate mapping reveals age-linked heterogeneity in naive T lymphocytes in mice. Proceedings of the National Academy of Sciences. 2015;112(50):E6917—-E6926. doi:10.1073/pnas.1517246112.

23. Hogan T, Yates A, Seddon B. Generation of Busulfan chimeric mice for the analysis of T cell population dynamics. Bio-protocol. 2017;4(24).

24. Hogan T, Yates A, Seddon B. Analysing temporal dynamics of T cell division *in vivo* using Ki67 and BrdU co-labelling by flow cytometry. Bio-protocol. 2017;7(24).

25. Verheijen M, Rane S, Pearson C, Yates AJ, Seddon B. Fate Mapping Quantifies the Dynamics of B Cell Development and Activation throughout Life. Cell Reports. 2020;33(7):108376. doi:10.1016/j.celrep.2020.108376.

26. Rane S, Hogan T, Seddon B, Yates AJ. Age is not just a number: Naive T cells increase their ability to persist in the circulation over time. PLoS biology. 2018;16(4):e2003949. doi:10.1371/journal.pbio.2003949.

27. Rane S, Hogan T, Lee E, Seddon B, Yates AJ. Towards a unified model of naive T cell dynamics across the lifespan. eLife. 2022;11:11. doi:10.7554/eLife.78168.

28. Lukas E, Hogan T, Williams C, Seddon B, Yates AJ. Quantifying cellular dynamics in mice using a novel fluorescent division reporter system. Frontiers in Immunology. 2023;14. doi:10.3389/fimmu.2023.1157705.

29. Sasaki K, Murakami T, Kawasaki M, Takahashi M. The cell cycle associated change of the Ki-67 reactive nuclear antigen expression. Journal of Cellular Physiology. 1987;133(3):579–584.

30. Miller I, Min M, Yang C, Tian C, Gookin S, Carter D, et al. Ki67 is a graded rather than a binary marker of proliferation versus quiescence. Cell Rep. 2018;24(5):1105–1112.e5.

31. De Boer RJ, Yates AJ. Modeling T Cell Fate. Annu Rev Immunol. 2023;41:513–532. doi:10.1146/annurev-immunol-101721-040924.

32. Costa Del Amo P, Debebe B, Razavi-Mohseni M, Nakaoka S, Worth A, Wallace D, et al. The Rules of Human T Cell Fate in vivo. Front Immunol. 2020;11:573. doi:10.3389/fimmu.2020.00573.

33. De Boer RJ, Perelson AS. Quantifying T lymphocyte turnover. Journal of Theoretical Biology. 2013;327:45–87. doi:10.1016/j.jtbi.2012.12.025.

34. Schittler D, Allgöwer F, De Boer RJ. A new model to simulate and analyze proliferating cell populations in BrdU labeling experiments. BMC Syst Biol. 2013;7 Suppl 1:S4.

35. Akondy RS, Fitch M, Edupuganti S, Yang S, Kissick HT, Li KW, et al. Origin and differentiation of human memory CD8 T cells after vaccination. Nature. 2017;552(7685):362–367.

36. Zarnitsyna VI, Akondy RS, Ahmed H, McGuire DJ, Zarnitsyn VG, Moore M, et al. Dynamics and turnover of memory CD8 T cell responses following yellow fever vaccination. PLoS Comput Biol. 2021;17(10):e1009468. doi:10.1371/journal.pcbi.1009468.

37. Seddon B, Tomlinson P, Zamoyska R. Interleukin 7 and T cell receptor signals regulate homeostasis of CD4 memory cells. Nature Immunology. 2003;4(7):680–686.

38. Pepper M, Linehan JL, Pagán AJ, Zell T, Dileepan T, Cleary PP, et al. Different routes of bacterial infection induce long-lived TH1 memory cells and short-lived TH17 cells. Nat Immunol. 2010;11(1):83–9.

39. Vehtari A, Gelman A, Gabry J. Practical Bayesian model evaluation using leave-one-out cross-validation and WAIC. Statistics and Computing. 2017;27(5):1413–1432. doi:10.1007/s11222-016-9696-4.